2011

Design And Integration Of System Components For A High Heat Flux Thermal Loop

Alvin Gregory Davis
North Carolina Agricultural and Technical State University

DESIGN AND INTEGRATION OF SYSTEM COMPONENTS FOR A HIGH HEAT FLUX THERMAL LOOP

by

Alvin Gregory Davis

A thesis submitted to the graduate faculty
in partial fulfillment of the requirements for the degree of
MASTER OF SCIENCE

Department: Mechanical Engineering
Major: Mechanical Engineering
Major Professor: Dr. John Kizito

North Carolina A&T State University
Greensboro, NC
2011

School of Graduate Studies

North Carolina Agricultural and Technical State University

This is to certify that the Master's Thesis of

Alvin Gregory Davis

has met the thesis requirements of
North Carolina Agricultural and Technical State University

Greensboro, North Carolina
2011

Approved by:

Dr. John Kizito Major Professor	Dr. Gary Tatterson Committee Member
Dr. Mannur Sundaresan Committee Member	Dr. Samuel Owusu-Ofori Department Chairperson

Dr. Sanjiv Sarin
Interim Associate Vice Chancellor for
Research and Graduate Dean

DEDICATION

I dedicate this thesis to my family for all of their support in helping me get to this point in my life. I thank them for teaching me that it is sometimes better to listen than be heard and to be willing to take criticism. Also, for helping me grow mentally and spiritually, along with allowing me to further my knowledge first hand. Finally, for their unwavering love and continuous encouragement, no matter what path I choose.

BIOGRAPHICAL SKETCH

Alvin Gregory Davis was born on June 17, 1986, in Durham, NC. He received the Bachelor of Science Degree in Mechanical Engineering from North Carolina Agricultural and Technical State University in 2008. He is a candidate for the M.S. in Mechanical Engineering.

ACKNOWLEDGMENTS

I would like to acknowledge my group members for all their insight and knowledge in helping me complete this research. Also, I acknowledge my advisor, Dr. John Kizito, for all his support in developing a plan of action and encouraging me to seek higher education. I would also like to thank Mr. Bruce Howe for his excellent machining services and insight into the design of the components for my experimental setup. Professor Daniel Acree also played an invaluable role in the completion of my research with his help in the initial design and selection of the components. In addition, I am grateful for the financial support from the Air Force Research Laboratory at Dayton, Ohio.

TABLE OF CONTENTS

LIST OF FIGURES

FIGURE **PAGE**

LIST OF TABLES

TABLE **PAGE**

LIST OF SYMBOLS

ρ	density $\left(\frac{kg}{m^3}\right)$
c_p	specific heat $\left(\frac{kJ}{kg \cdot K}\right)$
$\dot{m}$	mass flow rate $\left(\frac{kg}{\min}\right)$
$\dot{q}$	Heat flux $\left(\frac{W}{cm^2}\right)$
$\dot{Q}$	Heat transfer rate (W)
h_{fg}	Latent heat of Vaporization (kJ/kg)
T_{sat}	Saturation Temperature $(°C)$
V	Voltage (V)
k	Thermal conductivity $\left(\frac{W}{m \cdot K}\right)$
P	Pressure (MPa)
$\dot{V}$	Volumetric Flow Rate $\left(\frac{l}{\min}\right)$
t	time (min)
~~V~~	Volume (ft^3)

ABSTRACT

Davis, Alvin Gregory. DESIGN AND INTEGRATION OF SYSTEM COMPONENTS FOR A HIGH HEAT FLUX THERMAL LOOP. (**Major Advisor: John P. Kizito**), North Carolina Agricultural and Technical State University.

The goal of the present work was to develop a spray cooling heat transfer loop. The specific objectives were to facilitate a component-by-component design necessary to develop a spray cooling loop and to integrate these components into a system with a capability to remove a high heat flux of at least 1000 W/cm^2 from a heated surface. The system heater was characterized by developing a maximum heating curve at a specified minimum and maximum flow rates. In addition, a relationship between the mass flow rate and the applied pressure was developed. The design was tested to determine whether a cyclone could adequately separate two phase flow mixture supplied at the cyclone entrance. Finally, the main system pump was characterized by determining the pump-generated flow rates which were measured using flow meters located directly before the fluid entered the cooling chamber and expressed as a function of the input parameters.

The experimental test resulted in a maximum liquid flow rate of 0.95 L/min, which corresponded to a heat flux of 1,267 W/cm^2 and a steady state surface temperature of 824°C. The lowest liquid flow rate permissible was found to be 0.75 L/min and deemed to be an inefficient cooling flow rate because the cartridge heater wires began to glow red requiring the system be shutdown when the surface temperature reached 896°C. In addition, through experimentation, a relationship that described the effect of two-phase flow mixtures as a function of the nozzle type and spray pattern was developed.

CHAPTER 1

INTRODUCTION

The goal of present work was to develop a two-phase spray cooling heat transfer loop capable of removing a heat flux of 1000 W/cm^2 from a 1 cm^2 heated surface using water as the working fluid. From an extensive review of spray cooling literature, it was further realized that there was a lack of information on the design of two-phase spray cooling heat transfer loop designs. The objectives for the present work were derived from the need for a spray cooling heat transfer loop capable of testing the validity of the two-phase spray cooling technique found in previous spray cooling studies. Therefore, the specific objectives of the present study were to:

1. Facilitate the design and selection of components necessary to develop a two-phase spray cooling heat transfer loop

2. Integrate components into a system which can remove a high heat flux of 1000 W/cm^2 from a 1cm^2 heated surfaces by means of a two-phase spray cooling method

These objectives were determined to be necessary to achieve the goal of removing 1000 W/cm^2 from a heated substrate. The system requirements were set as:

1. The system had to be able to reach a steady-state temperature at the maximum heat flux.

2. The system had to supply a sufficient amount of fluid to cause the heater to reach a steady-state temperature at the maximum heat flux.

3. The system had to separate the two-phase fluid into its individual liquid and vapor components.

4. The system had to remove a sufficient amount of energy from the fluid to reduce the fluid temperature.

5. The entire system had to be capable of removing the maximum heat flux.

The thesis is organized as follows: The literature review necessary for the development of a thermal loop is presented in chapter two. The methods and materials used to design the loop are presented and discussed in chapter three. Then in chapter four, the results are presented and discussed. Finally, the conclusion and further recommendations for the present design are made in chapter five.

CHAPTER 2

LITERATURE REVIEW

In this chapter, a discussion on past and current literature based knowledge on spray cooling heat transfer loop designs is presented. The chapter is divided into different sub-sections based on the ultimate goal of the present study. These sub-sections focus on spray angle and surface to orifice distance, visualization systems, multi-nozzle setups, surface roughness, and other spray cooling methods. Table 2.1 presents a brief summary of the papers reviewed and the pertinent information gathered from each, such as maximum and minimum temperatures, heat flux, flow rate, and the working fluid used therein. The information obtained from the literature review was used to develop the specific objectives of the present study and to aid in design and selection of components used in the building of the thermal loop.

2.1 Effect of Spray Angle and Surface-to-Orifice distance on CHF

Visaria and Mudawar (2009) described the effects the spray angle and surface-to-orifice-distance have on critical heat flux (CHF) in a two-phase flow loop as shown in Figure 2.1. The authors of this work presented how overlapping sprays can decrease the CHF. The authors also developed a numerical model to determine the effects of inclined and normal spray patterns on the CHF. The angled spray nozzles result in non-uniform distribution of coolant, thus leading to a non-uniform cooling effect.

Table 2.1 Summary of the Literature Review

Author	Year	Max/min temp (^oC)	Max heat flux (W/cm^2)	Volumetric max/min flow rate	Working fluid
Visaria & Mudawar (2009)	Nov-08	77/22	N/A	23.9/3.33 m^3/s	Water, FC-72, FC-77, FC-87, PF-5052
Griffin, Vijayakumar, Chen, Sundaram, & Chow, (2008)	Nov-08	64.9/63.9	N/A	N/A	FC-72
Park, Vallury, Zuo, Perez, & Rogers, (2007)	Jul-07	60/8	30	1.2 l/min	Water
Lin & Ponnappan, (2003)	Apr-03	82.4/42	500+	N/A	Water, FC-87, Methanol, FC-72
Yang, Chow, & Pais, (1996)	Aug-96	100/20	1000	3/0.5 l/hr	Water
Horacek, Kiger, & Kim, (2005)	Dec-04		250	50 mL/min	FC-72
Fabbri, Jiang, & Dhir, (2005)	Jan-05	80	300	81.56/50.56 ml/min	Water
Pautsch & Shedd, (2005)	Apr-05	26/80	77.8	4.83/0.12 ml/s	FC-72
T. Shedd et al, (2005)	Apr-05				Nitrogen Saturated FC-72
Oliphant, Webb, & McQuay, (1998)	Mar-98	49.2/11.6	N/A	1.8/0.8 l/min	Air, Water
Mudawar & Estes, (1996)	Aug-96				FC-72, FC-87
W. Jia et al, (2002)	Dec-02	155/50	160	N/A	Water, Water Solutions
Nikolopoulos, Theodorakakos, & Bergeles, (2007)	Aug-06	210/25	140,000	N/A	n-Heptane, Water
Sally Sellers et al, (2008)	May-08	200			
Chen, Chow, & Navedo, (2004)	Aug-04	132.7/129.2	708.1	N/A	Water
Selvam, Lin, & Ponnappan, (2006)	Jul-06	N/A	N/A	N/A	N/A
C. C. Hsieh & Yao, (2006)	Sep-06	25/12	115,386		R-134a
Timothy Shedd, (2005)	‚Jun-05	N/A	150	2/1 L/min	FC-72
Lanchao Lin et al (2006)	Mar-06	N/A	430 w/o ejector, 500 with	0.63/0.30 gallons/min	Water, FC-72, FC-77, FC-87, PF-5052
Chizhov & Takayama, (2004)	Apr-03	600/70	N/A	N/A	Nitrogen
Ortiz & Gonzalez, (1999)	Dec-98	76/30	375, rough surface, 76 deg sub-cooling and Downward impact angle	2.91/1.48 l/hr	Water
Amon, Yao, Wu, & Hsieh, (2005)	Jan-05	60/-70	45	33.2/11.1 g/cm^2 min	HFE-7200
C. C. Hsieh & Yao, (2006)	Nov-05	80	50	4.41/0.19 g/cm^2 min	Water
Coursey, Kim, & Kiger, (2007)	Aug-07	95/55	60	123/69 ml/min	PF-5060
Kim, You, & Choi, (2004)	Mar-04	80/0	20,000	2.40/1.25 ml/min	water

The system design consists of a reservoir that holds the majority of the fluid. From the reservoir, the fluid travels to a chamber that deaerates the fluid at the beginning of the test and is used to maintain a set temperature of the coolant during testing. After the de-aeration, chamber the fluid travels through dual pumps which allow for greater fluid volume control. Next, it travels though a filter and into a pair of rotameters, then through a heat exchanger to create the desired heating chamber inlet temperature. Finally, it is injected into the chamber. The evaporated fluid travels through the condenser to the reservoir while the un-evaporated fluid travels directly to the reservoir as indicated in Figure 2.1.

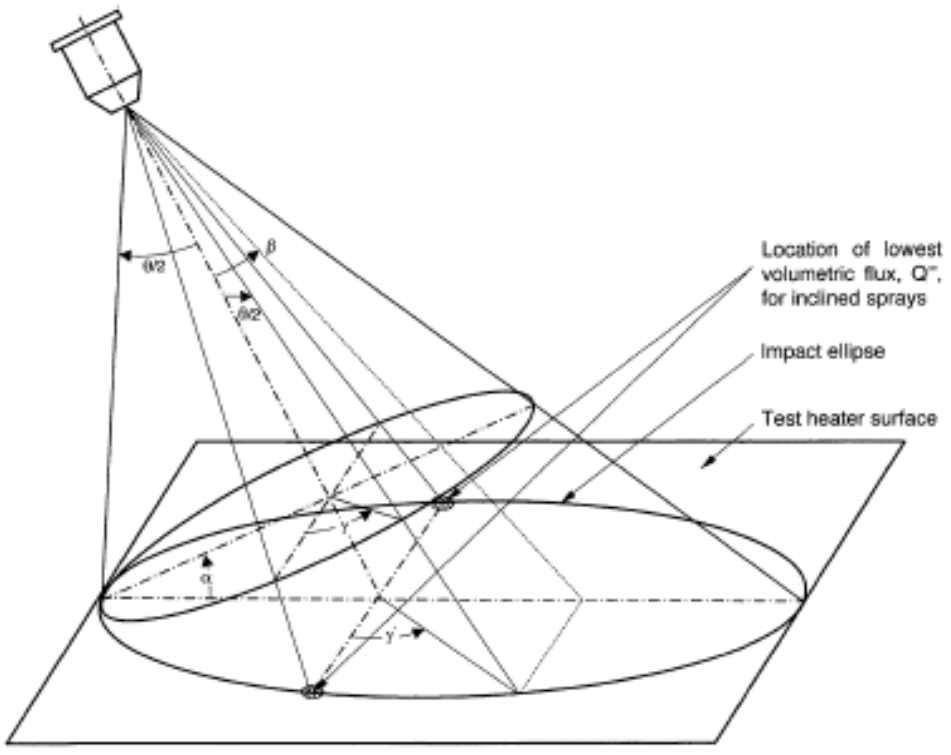

Figure 2.1. Schematic of angle nomenclature used in inclined spray model obtained from the study of Visaria & Mudawar (2009)

Mudawar and Estes (1996) described the effects of nozzle-to-surface distance and volumetric flux on the CHF. Their test chamber is shown in Figure 2.2. CHF was identified when the thermocouples being used detected a sudden unsteady rise in the heater temperature. The volumetric flux affects the CHF, in that, the maximum utilization of the spray flow rate is achieved when H (distance from nozzle to surface) is less than or equal to a parameter that relates the radius of a circle which inscribes the square heater surface (R) and the angle of the spray, θ.

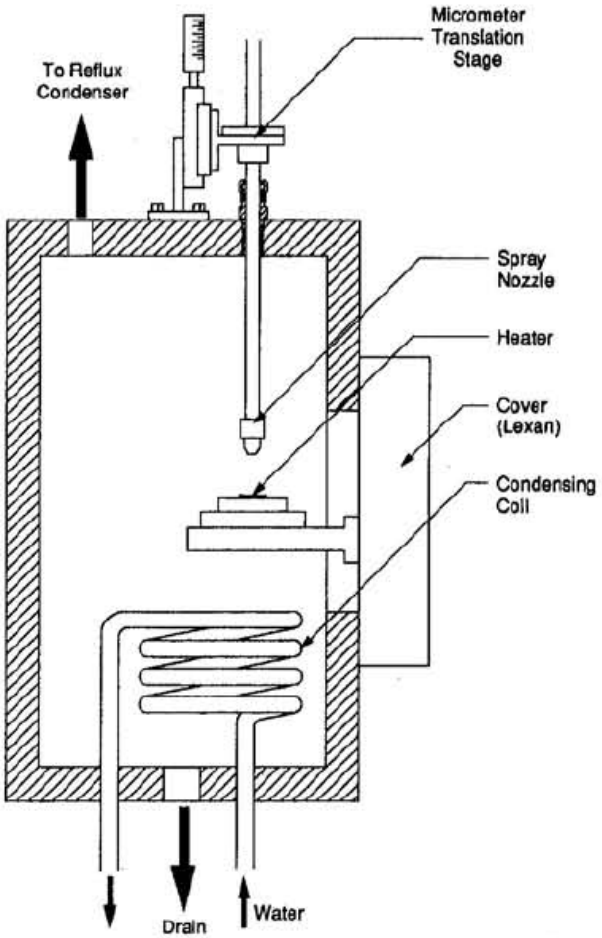

Figure 2.2. Schematic of the test chamber used in the study of Mudawar & Estes (1996)

From the experiments, it was determined that sprays which are located too far from the heater compared to those too close to the heater yielded small CHF. On the other hand, sprays that inscribed the heated surface produced the most efficient CHF. Also noted here was the fact that production of exact nozzles was nearly impossible, so selection of nozzle-to-surface distance should be done to maintain repeatability and predictability of the experimental results.

Rybicki and Mudawar (2006) presented a similar setup. The difference includes varying orientations and the use of PF-5052 as a working fluid in a downward-oriented spray compared to FC-72, FC-87, and water in an upward orientation. The data compares the effects of the nozzle, fluid, volumetric flux, droplet diameter, subcooling, and flow orientation. The system developed for the experimentation uses a pump to force the fluid through the heat exchanger, from the heat exchanger the fluid is moved into the upward facing spray chamber. From the spray chamber, the vaporized fluid moves into the reservoir and then into a condenser to be converted back into liquid; while the un-vaporized fluid flows directly into the reservoir, and then into the de-aeration chamber. Heating of a copper block is achieved by the use of nine 220W cartridge heaters, while the spray phenomena was visualized by the use of a transparent spray chamber made of G-10 fiberglass and polycarbonate plastic. From the data collected, it is determined that orientation has relatively zero effect on cooling performance, and proves that volumetric flux and sauter mean diameter are big influencers in the performance of spray cooling.

From the previous set of literature reviews discussing the effects of spray angle and surface to orifice distance, it was determined that there is a need for a way to adjust

the distance between the surface and orifice, but there is no need to change the orientation of the nozzle. The nozzle placement and orientation were very important in determining the final design.

2.2 Visualization Systems

2.2.1 Visualization of Bubble Propagation

Griffin, Vijayakumar, Chen, Sundaram, and Chow (2008) discussed the development of a system capable of measuring surface temperature while at the same time being able to visualize the bubble propagation process created during the pool boiling process. The surface temperature fluctuations are measured by thin film thermocouples while a high-speed camera was used to observe bubble propagation do to the heating of the fluid as shown in Figure 2.3.

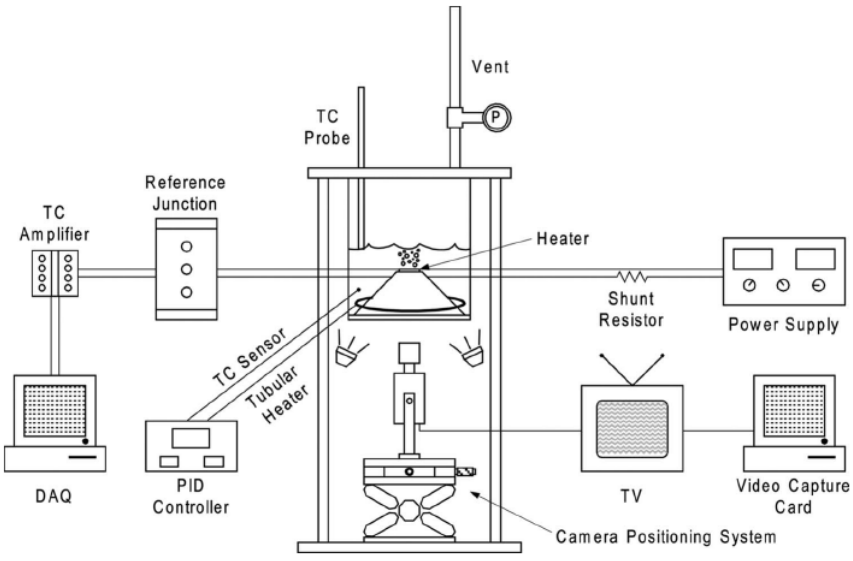

Figure 2.3. Schematic visualization of bubble propagation from the study of Griffin et al. (2008)

The heater was transparent by using a fused quartz base with a transparent layer of indium tin oxide for heating of the surface. The surface temperature was measured by copper-nickel thermocouples distributed throughout the substrate. From the data, they gathered that bubbles crossed the copper-nickel junction as the contact ring increased in size and then crossed back across the junction as it became smaller.

2.2.2 Visualization of Droplet Impingement

Horacek, Kiger, and Kim (2005) discussed the principal of using transparent reflection to take images of the impact of droplets on the heater surface (see Figure 2.4). The goal of this study was to determine the effect of dissolved gases on CHF. To visualize the effects an array of 96 serpentine platinum resistance heaters were fused onto a silica substrate allowing observation of the spray impinging onto the resistive heaters. They used a process called total internal reflection to record the impingement of the spray. The process requires passing a light through a right angle prism located under the silica substrate, and then the light reflected by the SiO_2 and vapor layer is captured by the camera.

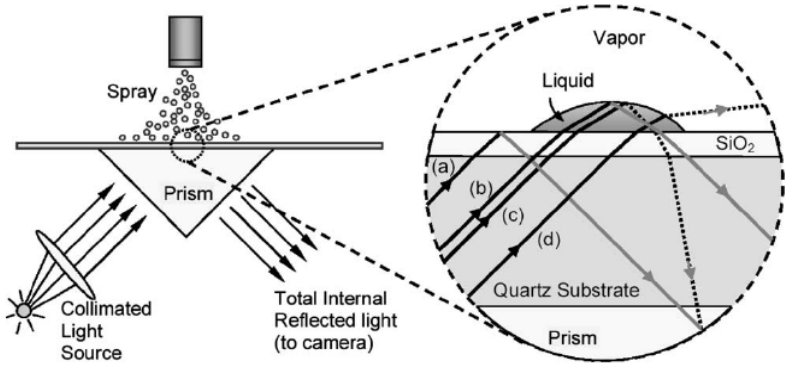

Figure 2.4. Schematic visualization of droplet impingement from the study of Horacek et al. (2005)

Horacek et al. concluded that non-condensable gases shifted the saturation temperature and increased the subcooling of the liquid. The work of Horacek et al. is relevant to the current study because the loop design is projected to operate with both a liquid and a non-condensable gas. The present study uses some of their research as a baseline to develop the two-phase loop required to cool the heated surface.

2.3 Effects of Multiple Nozzle Setups on CHF

Lin and Ponnappan (2003) described the use of a multiple nozzle setup and its effects on CHF. In addition, the authors discussed the performance of FC-72, FC-87, methanol, and water as choices of working fluids; along with the effects of non-condensable gases on the overall heat flux. The system developed consist of a magnetic gear pump, pre-heater, nozzles, and coaxial condenser. The system operates by pumping the liquid through the pump then through the pre-heater into a custom multi-nozzle plate with swirl inserts, from the nozzle plate the liquid is injected onto the heated surface and once the liquid is vaporized on the heated surface it then travels through the condenser and is converted back to liquid. The system proved that hybrid two-phase loops are capable of managing heat fluxes in excess of 50 W/cm^2.

Pautsch and Shedd (2005) also described the effect that multiple nozzles have on heat flux in their research on the effects of 1 through 16 swirl type nozzles on heat transfer (see Figure 2.5). According to the data, the performance of the nozzle was limited to the design which appeared to be the center for multi nozzle arrays due to nozzle overlap. CHF normally occurs near the edges where there is no continual flow of

fresh cooler fluid to keep the temperatures below critical values. The edge is also where the least mixing of the fluid happens due to the lack of droplets disturbing the free surface. According to the authors, CHF occurred before the surface of the die reached nucleate boiling. Therefore, the swirl inserts are of limited use due to lack optimal fluid distribution at the heated surface. On the other hand, their work indicates than more studies are still needed to improve fluid management and transport of the coolants from the hot surface to the thermal sink.

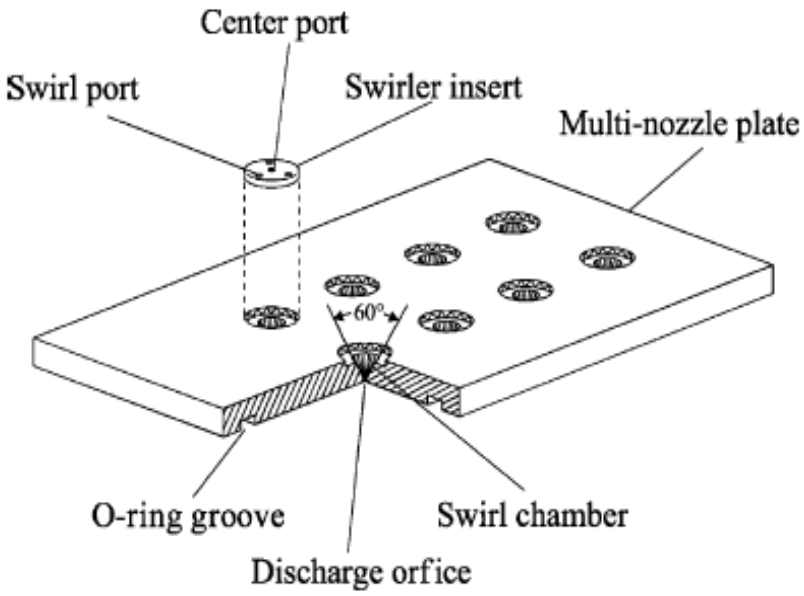

Figure 2.5. Schematic of the multiple nozzle setup from the study of Pautsch & Shedd (2005)

Shedd (2007) presented the development of a new nozzle layout that would increase thermal performance and peak heat flux, be scalable for large areas without

sacrificing performance and temperature uniformity, have better fluid management and maintain a small package volume. To do this, the author developed a multi nozzle setup that was adapted from microbore tubing; holes were drilled into the tubing at slight angles to produce fan type sprays. According to Shedd, their new design can achieve heat transfer coefficients from 1.6 $\frac{W}{m^2 \cdot K}$ to 2.4 $\frac{W}{m^2 \cdot K}$ at flow rates of 1 to 2 l/min with FC-72 as the working fluid.

2.4 Effects of Surface Roughness/Microstructures on CHF

Pais, Chow, and Mahefkey (1992) described the effects of different surface roughness on the heat flux of a copper block using water as the working fluid as shown in Figure 2.6. The figure illustrates the effect of surface roughness on vapor bubble generation and its interaction with an impinging spray. The paper details why greater surface area increases the heat flux achieved by increasing bubble propagation. Furthermore, the paper briefly compares the differences in heat removal between spray cooling and pool boiling to show that spray cooling is more efficient because it does not trap vapor on the surface of the heater. Pais et al. also discussed the use of tungsten-quartz tubular heat lamps as the heat source. Additionally, they describe the use of Constantan to improve the uncertainty of heat flux measurements when using thermocouples, normally caused by large spacing of the thermocouples. In conclusion, they determine that for air induced atomization nozzles, increasing liquid flow rate and air flow rate increases the heat flux.

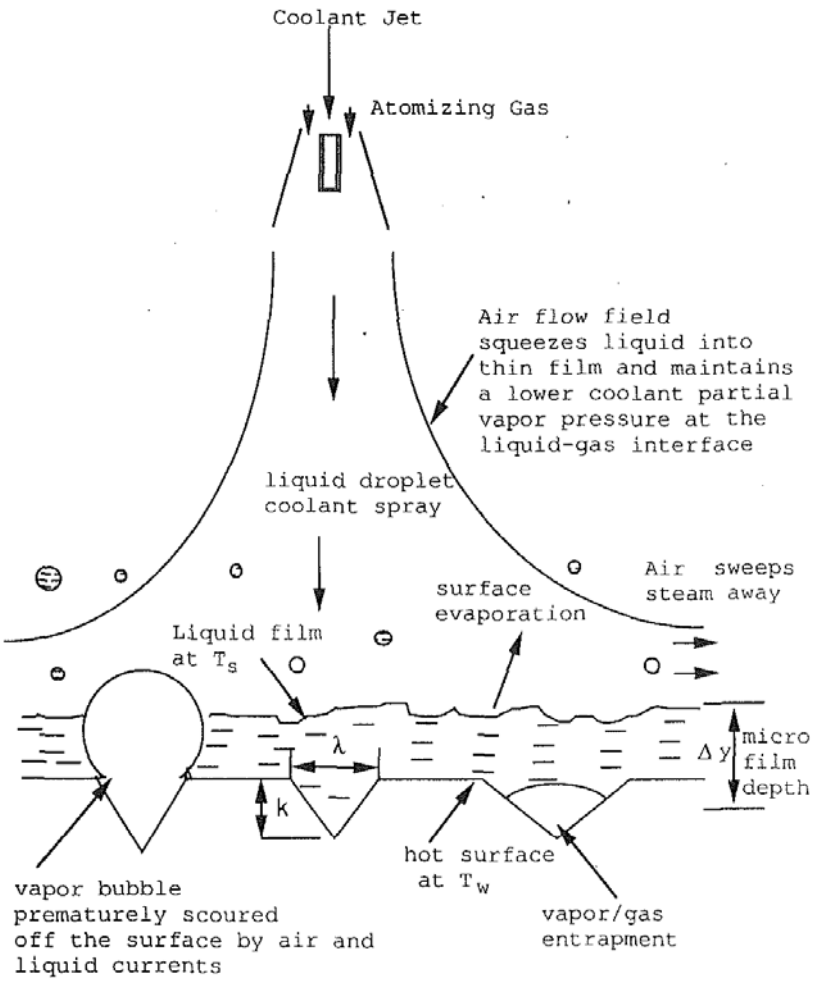

Figure 2.6. Schematic of how surface roughness creates bubbles. Obtained from Pais et al. (1992)

Bostanci, Rini, Kizito, and Chow (2009) presented results on the effects of spray cooling with ammonia on microstructures with protrusions, microstructures with indentations, and smooth surfaces. According to the data, the use of microstructures for heat removal showed an increase in performance compared to that of a smooth surface. For the protrusions, the heat removal increase was about 112% over that of a smooth

surface. On the other hand, for the indentations, the heat removal increase was about 49% over that of a smooth surface. The authors attributed the increase in heat removal to the increase in surface area.

Amon, Yao, Wu, and Hsieh (2005) discussed the development of micro-nozzles and micro-structures. The micro-nozzle design focused on droplet impingement, which would be used in evaporative cooling of electronics. The micro-structures focused on increasing thin film evaporation. Micro-nozzles of different shapes, size, and styles were tested for performance using HFE-7000 as the working fluid. For micro-surfaces different channel width and stud style were examined. The experimental setup consisted of testing a nozzle impingement cooling system, a micro-diaphragm liquid pump, coolant reservoir, and finned condenser. The authors concluded that while using a PC prototype as the test bed, they removed 45 W/cm^2 at a mass flux of 33.2 $\frac{g}{cm^2 \cdot \min}$.

Hsieh and Yao (2006) discussed the development of an experiment to determine the effects that micro-structures, different materials, system orientation and spray mass flux have on evaporative heat transfer characteristics. To determine the effect micro-structures had on evaporation, they compared three silicon chips with different surface textures (one with 120 μm Groove width and 160 studs, the second with the same groove width as the first but with 480 studs, and the third had 360 μm groove width and 480 studs) to a plain test chip and a polished aluminum plate. In addition to their baseline studies, they wanted to determine the effect of different spray mass fluxes. They used two different nozzles one with a mass flux of 1.50 $\frac{g}{cm^2 \cdot \min}$ for the low and 4.41

$\frac{g}{cm^2 \cdot \min}$ for the high mass flux. The test rig consisted of a rotary vacuum pump, a reservoir made of stainless steel to house the working fluid, which in this case was distilled water due to its high availability, and the two nozzles which they changed depending on the test condition (low or high mass flux). For the high mass fluxes cases, the chips where mounted on an aluminum plate heated by an aluminum block with four 500 W cartridge heaters attached. For the low mass fluxes, the aluminum heating block was replaced with 250 W mica foil heater. The focus area where the data was collected was a 25.2 x 25.2 mm^2 area. From this data, it was determined that the polished aluminum surface provided the highest heat transfer rate because of its more wettable surface property with water. Hsieh et al. further determined that the micro-structured surface performed best when the surface film thickness regimes are described as thin film or partial dryout. Additionally, during their experiments they discovered the effect the Bond number had on evaporation process. According to their data, the Bond number is the primary factor in evaporative cooling with micro-structures.

Coursey, Kim, and Kiger (2007) performed an experiment to determine the effects that different length fins on a heated surface have on heat flux, and the suitability for cooling electronics. The heater setup for their experiment consisted of one heater base with two 250 W cartridge heaters. A heater base was threaded to accept six detachable heads with a square surface area of 1.41cm x 1.41cm. Five of the detachable heads had fins of varying lengths and one had no fins, which was used as a control. Their overall loop consisted of a magnetic gear pump, nozzle, condensing coil, heat exchanger, and reservoir. The loop worked by pumping fluid through the nozzle onto the heated

surface where it was vaporized. The vaporized fluid would then collect on the condenser at the top of the spray chamber. Once condensed, the liquid would drop down through the bottom of the spray chamber. From the spray chamber, it would go through a heat exchanger to further reduce the temperature and then into a reservoir to begin the process again. The working fluid selected was PF-5060 due to its low boiling point of 56 °C at 1 atm. From their experiments, they determined that in a single phase case the optimum fin length is slightly longer than 5 mm and in the two-phase case this number decreased to about 1 mm in length.

Kim, You, and Choi (2004) experimented on the effects of air, water flow rate, and microporous coated surfaces on flat and cylindrical heaters. The experimental setup consisted of an airbrush mounted on a metal stand with a water dropper placed above the nozzle outlet, and a heated plate. The 5 cm x 5 cm flat plate heater was a copper block with nichrome wire as the heating element and the cylindrical heater was a copper tube with a 500W cartridge heater. From the results of the air jet test, they determined that the microporous surface increased the two-phase heat transfer compared to the plain surface. However, in the single-phase, there was no significant difference between the two surfaces. From their study of the plain and microporous surface for both the flat and cylindrical case, they determined that in both cases the microporous had better performance, and the only difference was the increase in the cylindrical case was not as drastic due to the decreased wetted area. The research determined that increasing the flow rate resulted in an increased heat flux in the heated substrate.

Ortiz and Gonzalez (1999) developed an experiment to determine the effects mass flow rate, surface roughness, subcooling temperature and impact angle on surface heat flux with two commercial nozzles. Flow rate for nozzle one had a maximum of 1.89 L/hr and minimum of 1.48 L/hr and for nozzle two the flow rate was 2.91 L/hr. From the mass flow rate data collected, it was determined that a higher CHF could be reached with the higher mass flow rate, possibly due to increase in water evaporation in their liquid thin film. After comparison of the surface roughness data, it was determined that the rough surface produced the highest CHF. In contrast, the smoother surface required a lower superheat allowing boiling to commence earlier than the rougher surface. For the subcooling comparison, a subcooling temp of 76 °C and 30 °C were compared. For the smooth surface as the subcooling temperature increases, the heat flux removal capacity decreases. For the rough surface, the CHF tended to be independent of subcooling degree. The data was collected at impact angles of 30, 45, and 90 degrees. It was determined that as impact angle increased, heat removal capacity decreased. The test rig was an open system consisting of a compressed air cylinder, pressurized water tank, in-line water heater, filter, temperature, pressure gauges, nozzle, and heated copper bar. From the data, it was determined that the maximum CHF increased with the mass flow rate and surface roughness, but decreased with subcooling on smooth surfaces and increasing impact angle.

2.5 Comparison of Spray Cooling and Other Methods of Heat Removal

Fabbri, Jiang, and Dhir (2005) compared the use of spray cooling versus the micro-jets to cool a microchip. Custom orifice plates were created for different numbers of jets for the micro-jet setup and a single HAGO nozzle was used for the comparative spray nozzle. De-ionized water was used for all the experiments. According to the data, the spray nozzle has a higher heat transfer rate at a lower flow rate compared to that of the jet setup. Also determined was that at the same pressure the micro-jets could remove as high as 240 W/cm^2 compared to the sprays 93 W/cm^2. This could be due to the single type of nozzle used in the comparison. The authors concluded that the micro-jet was successful since it removed 129 W and created a heat flux of 300 W/cm^2 at a surface temperature of 80 °C.

Oliphant, Webb, and McQuay (1998) also discussed the differences between spray cooling and multi jet cooling. They showed that sprays produced the same heat transfer coefficient as jets, but sprays did it at a much lower mass flux. Briefly discussed is the potential cause for the effectiveness of spray cooling. The spray cooling method is explained as being effective because of evaporative cooling and the thin film along the impingement surface. The film thickness ranges from 10 – 30 μm with a radial spread of 50 – 150 μm depending on whether the mass flux is low or high. Another contributing factor could be the expected unsteady boundary layer caused during spray impingement studies.

Park, Vallurym, Zuo, Perez, and Rogers (2007) discussed the use of the capillary effect and evaporators for the cooling electronics. They developed a system similar to a

single evaporator hybrid two-phase loop that consists of an evaporator, a condenser, reservoir, and a mechanical gear pump. The fluid is pumped from the reservoir, through the evaporator were the vaporized fluid exits through a vapor outlet on the top then through the liquid condenser and then into the reservoir. The fluid that was not vaporized goes directly from the evaporator to the reservoir. The only difference between theirs and the single evaporator is that they have four evaporators.

Another method proposed by Lin, Ponnappan, and Yerkes (2006) discussed the use of an ejector, which is used to reduce the effects of vapor entering into the magnetic gear pump further allowing for increased CHF. From their studies using water and FC-72, they determined that vapor that entered into the gear pump reduced the pumping pressure head or made it impossible for the pump to produce a pressure head. They created a two-phase loop with a cooling unit. The loop consisted of a pre-heater, spray chamber, 48 nozzle housing, heater assembly, condenser, ejector with bypass loop, magnetic gear pump, liquid reservoir, and filter. The fluid flows through the ejector into the pump, splits, half of the liquid going to the pre-heater then nozzles then to the condenser and back to the ejector while the other half goes directly back to the ejector. They concluded that the ejector prevents uncondensed vapor from entering the gear pump, which in turn enhances its pumping capabilities. With the use of the ejector, they produced a 16% increase in CHF compared to a system that does not utilize an ejector.

Hsieh, Fan, and Tsai (2004) focused their paper on the nucleate boiling aspect, when applied to spray cooling with working fluids water and R-134a. For their experimental studies, an 80 degree nozzle was used with a diameter of 0.38 mm. The

distance between the nozzle and the heater was fixed at 60 mm, which allowed for the entire surface of the copper block heater to be completely wetted. According to the authors, spray mass flux in terms of We, number has a strong effect on spray cooling performance, while the effects of sub-cooling are still unclear because of low sub-cooling. The authors also conclude from the data that water is a better working fluid for spray cooling compared to R-134a.

Mudawar, Bharathan, Kelly, and Narumanchi (2009) discussed the potential use of spray cooling in hybrid vehicles. Their objective was to dissipate heat flux range of 150-200 W/cm^2 and maintain a chipset temperature below 125 °C. Their paper also discussed differences between indirect and direct liquid cooling. Moreover, their study details the coolant selection process, which ends up recommending R134a as the best coolant and HFE-7100 as the best liquid coolant, based on a specific selection criteria. After describing the testing process, it is shown that the selected coolants are efficient at maintaining the temperature range within the required pressure for hybrid vehicle applications.

2.6 Effect of Liquid Droplets on CHF

2.6.1 Experimental Studies

Sellers and Black (2008) studied the effects of a single water droplet being dropped onto a heated plate. This author focuses on droplet size, speed at which droplet impinges onto surface, frequency, and location of the drop. The droplets impinge onto the surface by gravity; the droplet size range of 97–392 μm and placement are controlled

by a vibrating piezoelectric motor and two sets of charged orthogonal plates, respectively. For the testing two different types of heaters were tested, a nichrome thin-film heater and copper block heater. A total of 407 CHF tests were performed, 52 of those where performed with the nichrome heater, and of the 407 about, 10% where random repeats. CHF achieved in the study ranged between 24 – 297 W/cm^2 with surface temperatures between 117 and 130 °C.

Chen, Chow, and Navedo (2004) discussed the effects of droplet Sauter-mean diameter, d_{32}, droplet velocity, V, and droplet flux, N, on the efficiency of liquid usage (η) at CHF. From their experimentation, it was found that by varying one of these parameters and keeping the other two constant, the output (η) could vary. Furthermore, it was found that d_{32} has relatively no effect on the CHF. After all testing was completed, it was concluded that by using a nozzle that creates a small droplet diameter and has a high output velocity, the greatest CHF could be achieved with the smallest amount of water.

Hsieh and Tien (2007) also discussed the effect of spray droplet dynamics including that of impinging spray atomization. In addition, the spray impingement heat fluxes were obtained using R-134a as the working fluid in the non-boiling regime. The focus of their study was on the pre-impingement process, flow structure, and cooling capacity of the plate when linked to spray cooling. To visualize the droplet motion, a 140mm sight glass was installed in the chamber so that an LDV could be used. According to the author the Weber, *We* number has a strong effect on spray velocity characteristics, droplet size distribution, and Sauter-mean diameter while in flight.

2.6.2 Computational Studies

Tao, Huai, and Li (2009) discussed the computational setup for simulation of a water droplet impinging into a liquid film. The study details two different experiments, one with a vapor bubble growing in a liquid film and the other experiment is a spray impinging onto a thin film having a vapor bubble. The computational portion uses the Volume of Fluids (VOF) model to simulate both aspects. In the simulation of the vapor bubble growing with a water droplet impinging, one can see how a droplet impinging onto a liquid surface increases heat flux due to the fact that the spray quicken the distortion speed of the vapor bubble as well as created a secondary nuclei within the liquid film.

Nikolopoulos, Theodorakakos, and Bergeles (2007) discussed the use of the VOF method coupled with the Navier-Stokes equations to numerically simulate liquid droplet impingement onto a heated surface. The working fluids used were n-heptane for the first three 2D cases at different Weber numbers. In addition, for the 3D case, the working fluid was water. The author cites previous work that focuses on different types of liquid droplet impingement and they focus on the surface and/or atmospheric effects. Their paper also takes into account the heat flux before and after the Leidenfrost phenomenon. The numerical modeling at the interface was analyzed using an adaptive grid refinement technique which updated the grid every 20 iterations thus allowing for prediction of the flow characteristics before and after the Leidenfrost point. Also, discussed numerically is the shape deformation process in terms of spreading rate and height.

Selvam, Lin, and Ponnappan (2006) discussed the use of a computational method to determine droplet impingement. The computational technique is called the level set method to model multiphase flow. The method differs from the VOF method in the implementation of the technique but both can be used to solve similar problems. The problems were solved. One was a water droplet impinging on to a thin film with a vapor bubble imbedded. The other was a vapor bubble growing and merging with the vapor layer attached to a heated substrate. These studies were limited to a small diameter range. The computational study focused on the micro environment with a bubble diameter of 40 μm. The authors surmise that when the water droplet impinges onto the thin film away from the location where the vapor bubble is growing, the heat flux increases. On the other hand, when the water droplet lands on the location containing a vapor bubble, the heat flux does not change. The bubble breaking through the surface allows for the cooler droplet to get to the heated surface faster. In conclusion, by comparing the maximum average Nusselt number for both cases, it is noticed that when only phase change is present the maximum Nu is 50. In contrast, when there is a water droplet that breaks the thin film up, there is a maximum Nu of 160.

Chizhov and Takayama (2004) numerically examined the effects of a solid nitrogen droplet at 80K impinging onto a heated surface at 600K. From their research, they developed a relationship between droplet size and heat flux. It is determined that the heat flux depends on the velocity of the fluid droplet and size (1mm or less).

CHAPTER 3

METHODS AND MATERIALS

The focus of this chapter is to present the methods and materials that were used in the selection and assembly of the components in the spray cooling thermal loop shown in Figure 3.1. The figure shows a photograph of the actual loop layout together with the diagnostic tools and data acquisition system. The detailed description of the experimental setup and the diagnostic tools are discussed later.

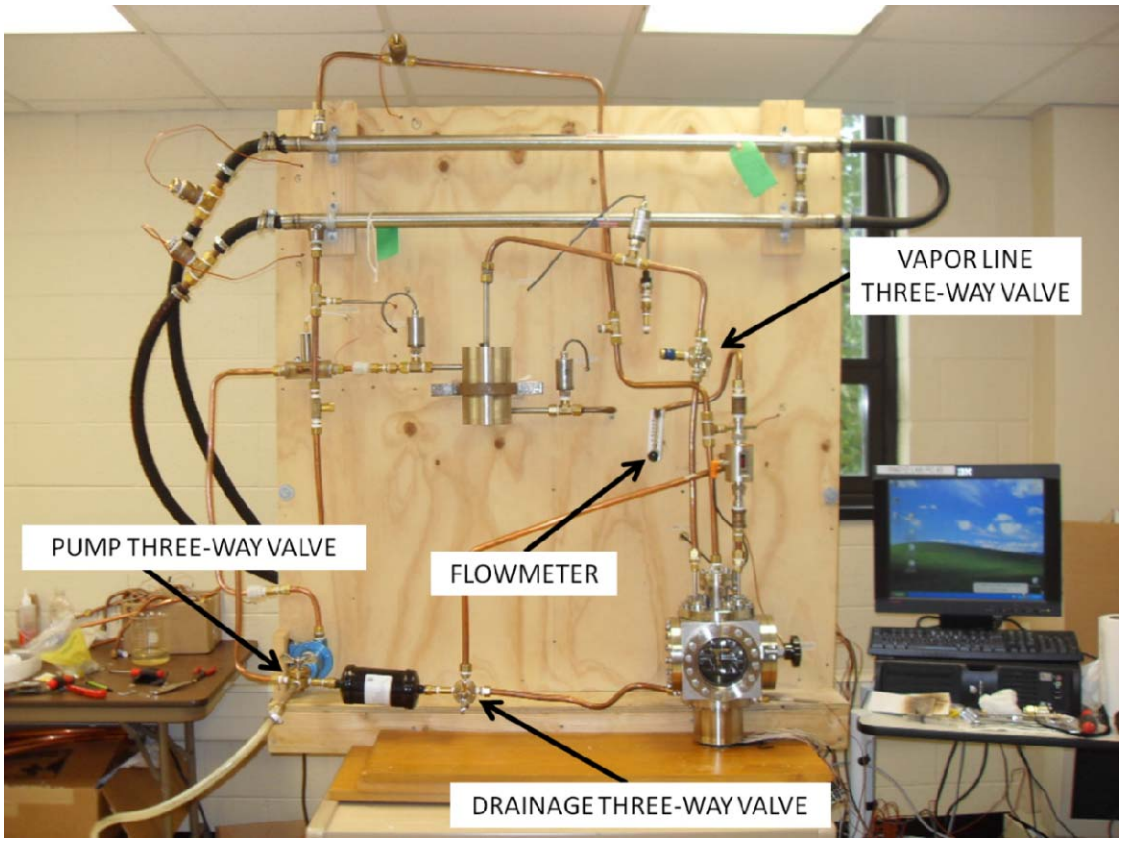

Figure 3.1. Finalized spray cooling loop design with installed components

3.1 Spray Cooling Loop Design

The spray cooling loop was designed with an ultimate goal of removing a heat flux of 1000 W/cm^2 from a heated copper surface using a two-phase spray cooling method. The two-phase method was adapted from the ammonia absorption refrigeration cycle. A refrigeration cycle is illustrated in Figure 3.2(a) and an absorption system is similarly illustrated in Figure 3.2(b). The two systems are similar with a major difference being that the compressor in the refrigeration system is replaced by the ammonia absorption system. The absorption process is described in detail by Çengel and Boles, (2002). The cycle is cited as an example to indicate the possibilities of operating a refrigeration system without a compressor but instead using a pump to increase the pressure between the heat sources and sinks.

For the current study, the parameters that were considered critical for the selection of the components were the pressure and temperature operation limits. These parameters also depended on the suppliers and vendors of the system components. The remainder of this section describes the processes taken to select the off-the-shelf components, the process taken to design in-house components, and then devised the procedures necessary for the integration process. The final system was required to have the components work together as a unit.

3.1.1 Two-Phase Flow Loop

To build a two-phase heat transfer loop capable of removing high heat fluxes, the system components must be capable of meeting the entire system requirement outline in

Chapter One. The system developed consisted of a pump, cyclone, reservoir, injector chamber, heating chamber, heat exchangers, and a chiller.

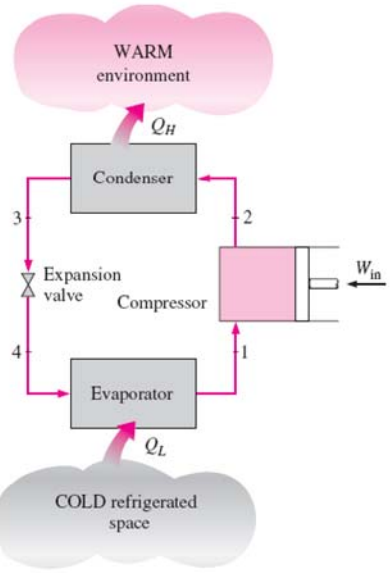

(a)

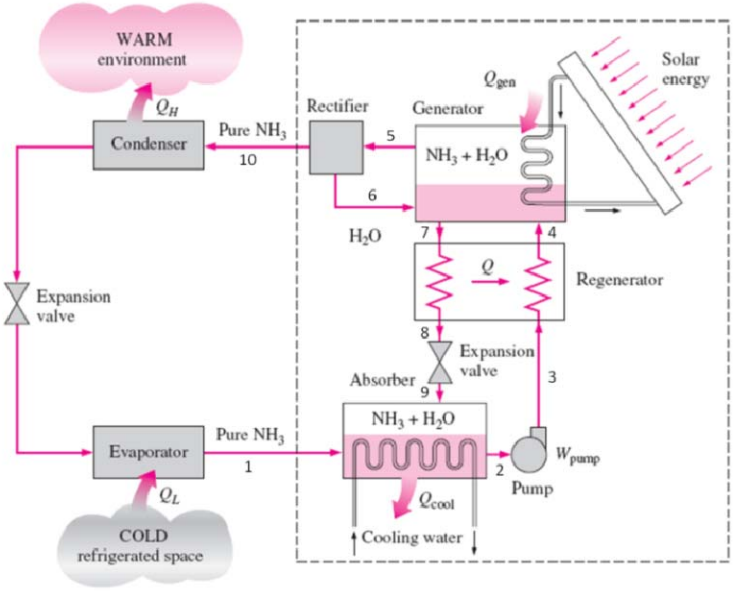

(b)

Figure 3.2. (a) Refrigeration cycle, (b) Ammonia cycle obtained from Çengel & Boles (2002)

The initial development of the loop consisted of many iterations to determine the component need, placement, and function in the overall loop. Through all the design iteration of the loop, majority of the components remained in the same location as illustrated in Figure 3.3 and Figure 3.4. Figure 3.3 is the initial design layout with the pump located after the cyclone. The layout was modified to change the location, the number of pumps, and the type of pump as illustrated in the component layout in Figure 3.4.

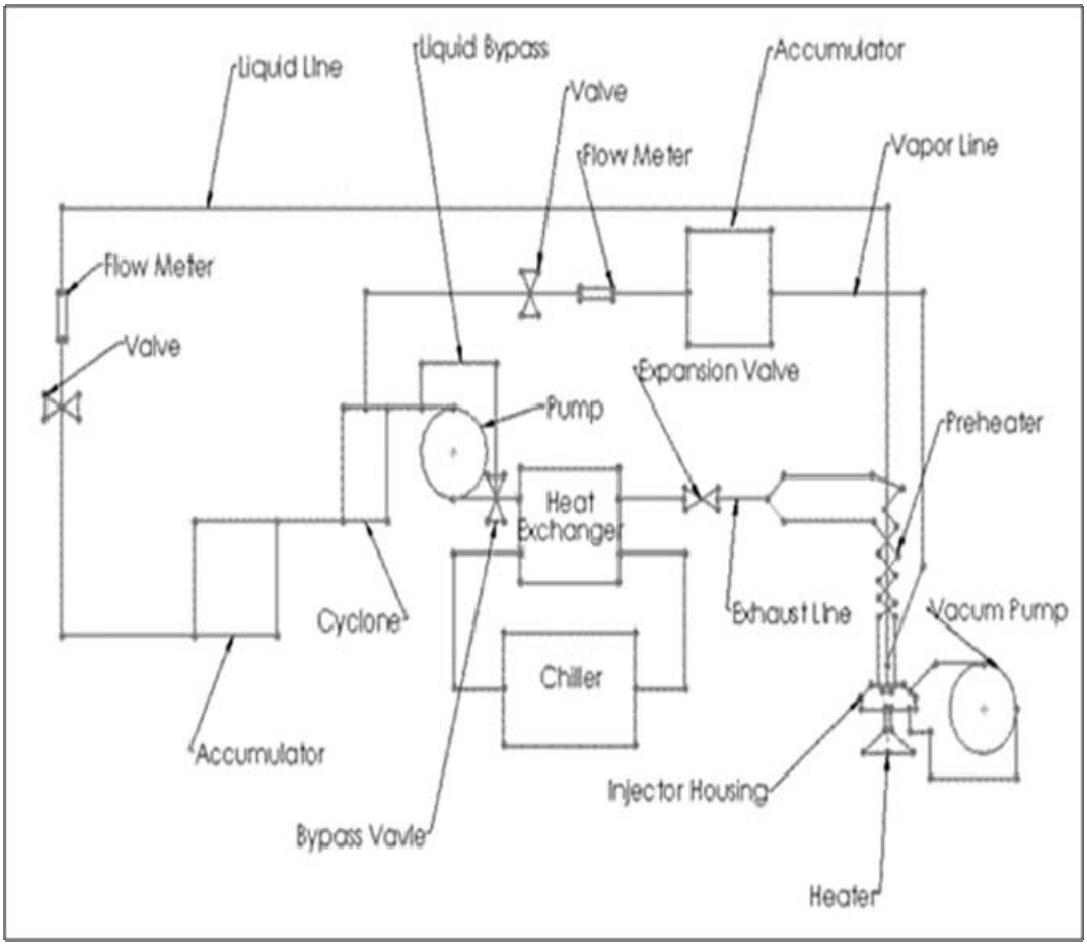

Figure 3.3. Initial component layout

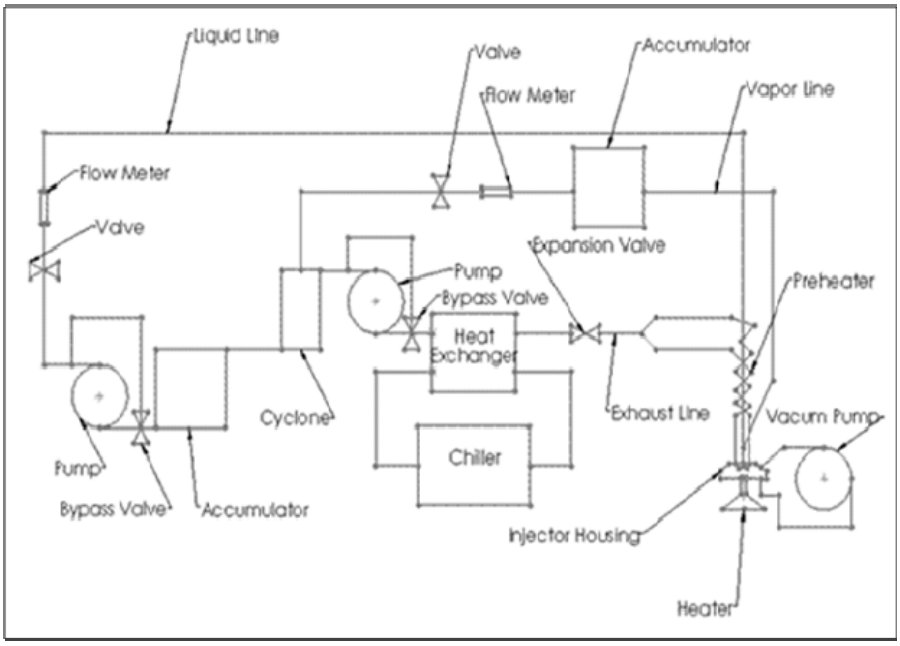

Figure 3.4. Modified component layout

The final iteration results of component layout are shown in Figure 3.5. The final layout was derived as a result of the available components, the integration process, and the stability of the system. Under steady state conditions, the system is intended to operate by compressing the two-phase mix through the rotary pump. The pressurized fluid is then introduced into the cyclone from the pump. The cyclone has two exits and it is designed to separate the two-phases into two distinct phases as will be explained in detail later. The liquid phase from the cyclone has two paths depending on the metering requirements at the cone nozzle. One path leads the fluid to an overflow reservoir and the other leads the fluid to a cone nozzle. The vapor phase from the cyclone is routed to the cone nozzle where the vapor phase is mixed with the liquid phase. The mixture atomizes upon exit from the cone nozzle. The atomized fluid can now be described as a

spray. The spray characterization will be described later. The spray from the cone nozzle impinges onto the heated surface where it is supposed to completely vaporize and exit through the top of the heater chamber and enters the heat exchanger. Initially, the loop was designed to meter the correct amount of fluid required to completely vaporize thus maintain constant temperature at the heated surface. The design required no drainage of excess fluid. The no drainage condition was difficult to achieve. Therefore, in the second modification the fluid that would not vaporized is allowed to drain through the bottom of the injector chamber and is re-introduced before the pump as depicted in Figure 3.5.

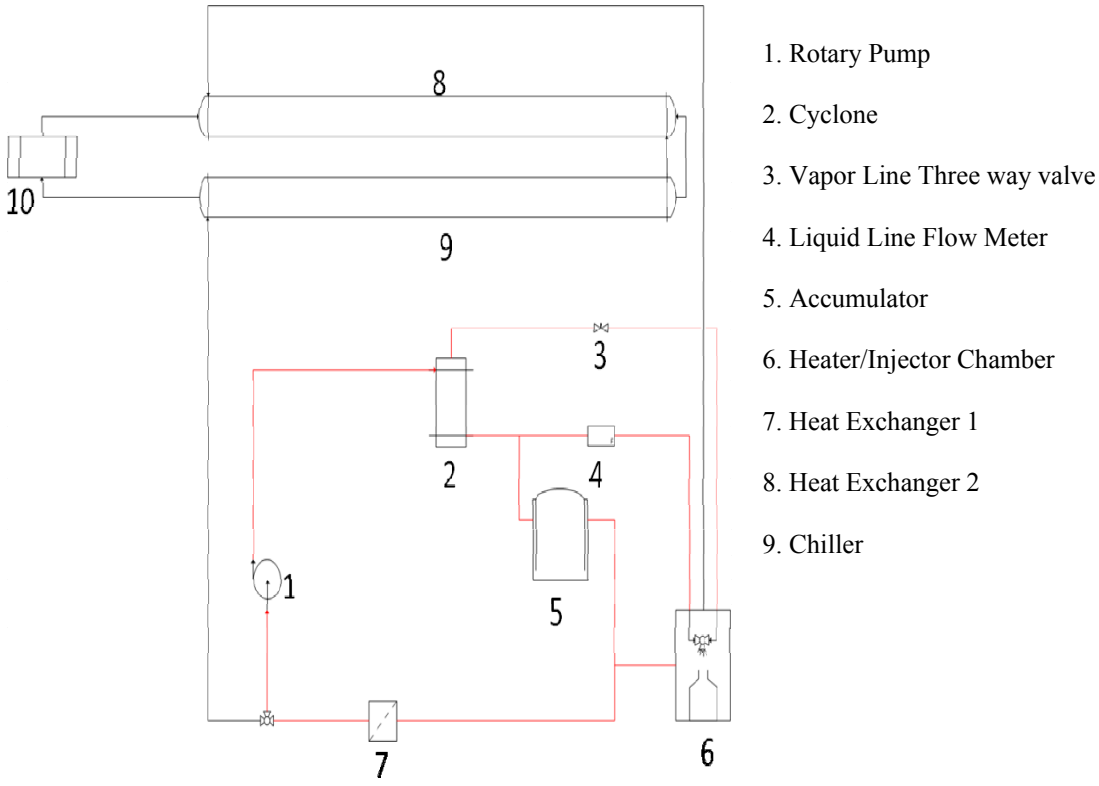

Figure 3.5. Final design layout

The efficiency of atomization depends on the amount of separation that occurs within the cyclone and the mixing process right before the injector. The injected fluid-vapor mixture, whose temperature is at T_{sat}, impinges onto the heated surface and is then vaporized, thus increasing the pressure in the chamber. The super heated vapor is then flows to the heat exchanger, where energy from the vapor is transferred to the ethylene glycol loop provided by the chiller. The heat exchanger condenses the vapor back to a two-phase mixture at T_{sat}. The system operation parameter must be tuned such that all components, such as the pump flow rate and chiller temperature are capable removing at a minimum 1000 W/cm^2 from the system. A simplified schematic of the heat transfer loop is depicted in Figure 3.6.

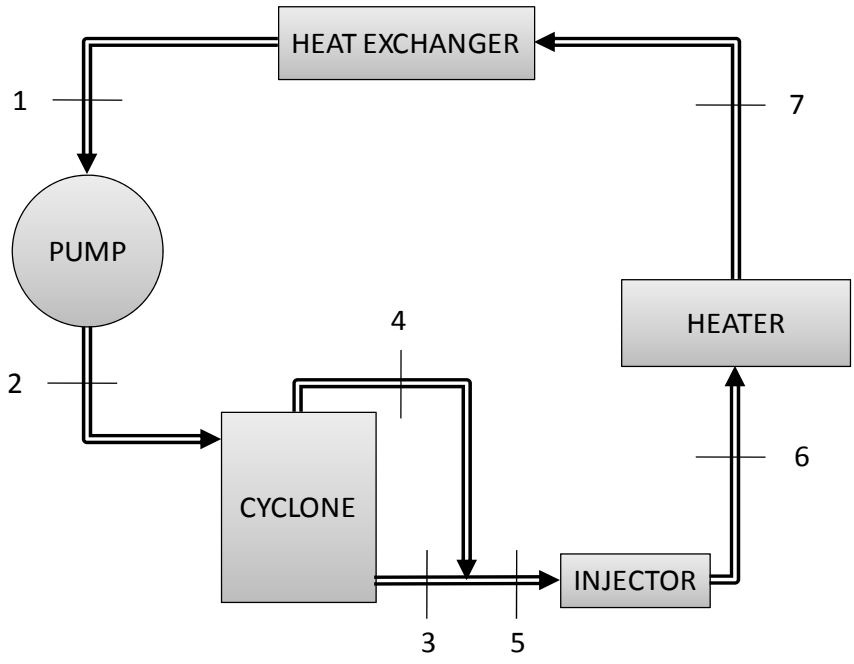

Figure 3.6. Simplified component layout

3.1.2 Spray Cooling

Spray cooling is a very effective method as a high heat flux removal tool that has use in various applications where systems capable of achieving heat fluxes in excess of 1000 W/cm^2 (Yang, et al., (1996)). Spray cooling has been used in applications ranging from the cooling of high speed electronics to cooling of steel in industrial roll out mills. There are many different methods to cool using spray techniques including evaporative cooling, jet impingement cooling, and micro-droplets as discussed in Chapter Two. Any cooling technique has its own pros and cons based on the intended application. The main reason for using spray cooling as opposed to jet cooling would be because jet cooling is prone to flooding at the heated substrate. Secondly, sprays have the ability to increase the surface area of the liquid phase. The present study chooses the spray cooling method because of the aforementioned reasons.

3.1.3 Working Fluid

Selection of the working fluid is one of the most critical components in the design of a thermal loop, because of its influence the following parameters:

1. Types of materials selected
2. Type of components used
3. The maximum heat flux achievable
4. The temperature and pressures at which the loop functions

The remainder of the section focuses on the possible working fluids.

Latent heat of vaporization (h_{fg}) which is defined as the energy required to vaporize a fluid. Latent heat of vaporization was determined to be main parameter used

to select the working fluid. A few other parameters that were made note of are the following properties: flammability, dielectric properties and toxicity.

Before the list of parameters was focused on, a list of potential fluids was developed. The list consisted of the most commonly used fluids as presented in Table 3.1.

Table 3.1. Working fluid characteristics

Fluid	T_{sat} (°C)	h_{fg} (kJ/kg)	Flammability	Dieletric	Toxic
Water	100.0	2257.0	NO	N/A	NO
R-134a	-26.1	216.8	NO	N/A	LOW
Ethanol	78.2	838.3	YES	N/A	HIGH
Ethylene Glycol	198.1	800.1	YES	N/A	LOW
Novec-7000	34.0	142.0	NO	YES	LOW

From Table 3.1, it is seen that the best working fluid would be Novec-7000 due to the combination of two factors which are the low boiling point and low flammability. Even though R-134a has a lower boiling point than Novec-7000, requires special containment, disposal, and licensure. For the experiments performed in the present research, water was used as the working fluid because of the lack of a facility with proper ventilation to properly handle toxic fluids. The major downside of working with water is its high boiling point. The biggest advantages of water as a working fluid are the large latent heat of vaporization and that water is ubiquitous. In two phase flow system used for heat transfer, large amounts of heat energy are transferred without increased

temperature at the substrate. Normally the substrate remains at boiling point until the liquid phase is consumed.

3.1.4 Nozzle Types

The type of nozzle used in a spray cooling application has a large impact on the overall heat flux that can be achieved. Therefore, research has been done on how nozzles used in spray cooling applications influence heat flux. Research ranging from the size, style, number, and orientation of nozzles has been done to determine their effects on heat flux. To aid in the selection process, a decision matrix shown in Table 3.2. The matrix was developed to weigh the prospective nozzles against the desired function.

Table 3.2. Nozzles decision matrix

Criteria	Temperature	Pressure	Spray Shape	Flow Rate	Fluid Type	Total
Percentage	20%	20%	20%	30%	10%	
Cone						
Full Cone	5	5	5	5	5	5.0
Hollow Cone	5	5	2	3	5	3.8
Square	5	5	4	5	5	4.8
Atomization						
Swirl	4	5	1	4	3	3.5
Fogging	4	5	1	4	5	3.7
Misting	4	5	1	4	3	3.5

From Table 3.2, the nozzle that should be selected based on the criteria would be a full cone nozzle. The full cone was selected because it met all the design requirements. Even though the square cone nozzle came in a very close second, it was not selected

because the heat substrate was circular. This means that if the square cone inscribed the circle the whole surface would not be adequately covered, and if it was larger than the surface, a good portion of the fluid would be wasted. In summary, of the full cone nozzles available a 30, 60, and 90 degree angle nozzle were purchased for comparison and their influence on the heat flux.

3.1.5 Heater

As discussed in Chapter two, most experimental spray cooling loops use some form of heater to produce heat. The heaters simulate the real world heat generating application. Common heating element types are cartridge heaters, nichrome wire, thin film resistance heaters, and heating lamps. Most of the heater housings are manufactured from copper and aluminum, but copper is the most common because of its high thermal conductivity and high melting point compared to that of aluminum. The remainder of this section will focus on the processes taken to select the heater element, and heater material.

The development of the cooling loop began with the design and selection of the components for the heater, because the heat load drives the design. The design began with the material selection and sizing of the heater. The selection of fabrication material was between aluminum and copper as a result of their excessive use in previous research, for example, Visaria and Mudawar (2009) and Oliphant et al. (1998). The thermal properties in Table 3.3 also aided in the decision of the material to be used for the heater. From Table 3.3, and the information gathered from the vendor McMaster-Carr, the material selected was copper because of its ease of machinability, high melting point, and

high thermal conductivity. Once the material was selected, the next task was to size the heater. To size the heater, the billet sizes available from the supplier and number of heater elements were required to be known a priori.

Table 3.3. Material properties

Properties	Aluminum	Copper Alloy 101 (99.9%)
Melting Point (K)	933	1358
c_p (J/kg-K)	903	385
k (W/m-K)	237	401

Heater cartridges were selected because of their high power output, availability, and relatively small size. The heaters were procured from Omega Engineering, where it was determined that a total of sixteen ¼" x 2" 250 W cylindrical cartridge heaters were needed to supply the max 1000 W/cm^2 heat flux. Based on the cartridge dimensions, a 2" diameter by 5" tall copper billet was selected. A cylindrical billet was selected for ease of machinability. From these dimensions, initial designs of the heater were developed as seen in Figure 3.7 which depicts the different design iteration. The design shown in Figure 3.7(a) is simply a cone shape. This design was not selected because of the effort required to machine the long taper and bore the angled holes. The second design in Figure 3.7(b) was a modification of the initial heater design, but instead of having holes bored at an angle; a cylinder was placed at the bottom allowing the cartridge heaters to be mounted vertically.

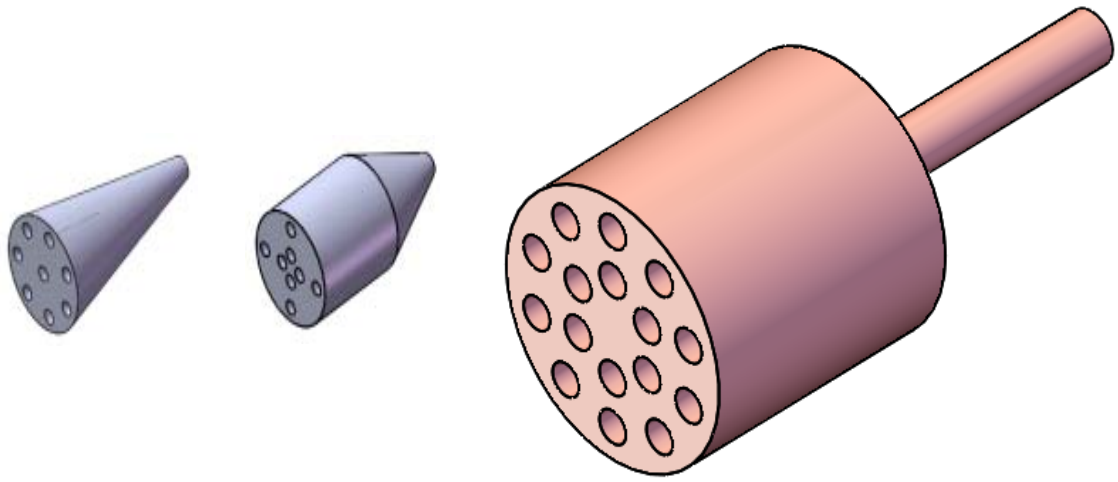

(a) (b) (c)

Figure 3.7. (a) Initial heater design, (b) Modified heater design, and (c) Final heater design

The final and selected design shown in Figure 3.7(c) consists of the same cylindrical design as the second design. Instead of tapering all the way to the top of the billet, it has only been tapered slightly and the rest is cylindrical. The design allows easier instrumentation. To be able to determine the heat flux, a series of holes were drilled vertically along the stem of the final heater. Since the thermal conductivity and the distance between any two points is known, the heat flux can be determined based on the heat flux equation by measuring the change in temperature between any two points.

3.1.6 Pumping System

The design of a spray cooling loop requires the proper selection of the pump type. The pump needs to be adequately sized to supply the desired amount of cooling. Majority of pumps used in closed loop spray cooling applications are mechanical gear

pumps, due to their ability to supply the desired flow rate and pressure. In situations where two-phases are present within the loop, the use of mechanical gear pumps has been shown to reduce pumping pressure head and can make generation of a pressure head impossible. As a result, the use of phase separators has been introduced to reduce this effect. A typical example of a phase separator is an ejector, which would remove the vapor from the mix before it enters into the pump. The rest of this chapter discusses the processes used in the selection of the pump for the spray cooling loop.

Now that the heater has been designed a pump capable of flowing two-phases and removing the heat flux was selected. Using the selection process outlined in Fox & McDonald, 1985, which states that the steps necessary to select a pump are to:

1. Select a supplier
2. Determine the required mass flow rate
3. Determine the required pressure head

To determine the required mass flow rate for the pump, an energy balance using equation 3.1 was performed with Figure 3.8 as the working diagram.

$$\dot{Q}_s = \dot{Q}_v - \dot{Q}_l \tag{3.1}$$

$$\dot{Q}_s = \dot{m}_v h_{fg} - \dot{m}_l c_p \Delta T \tag{3.2}$$

$$\dot{m} = \frac{\dot{Q}_s}{h_{fg} - c_p \Delta T} \tag{3.3}$$

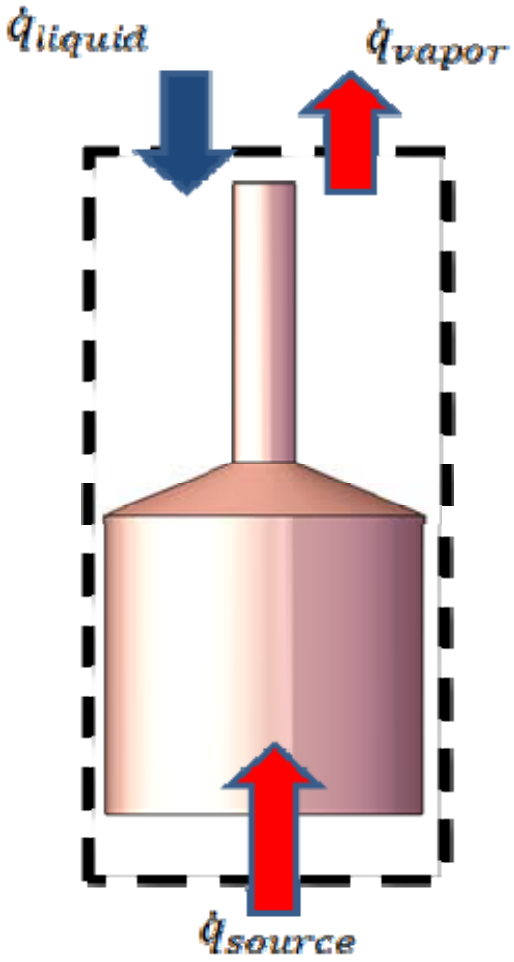

Figure 3.8. Free body diagram of heater in control volume

Given the fact that majority of pumps are specified in volumetric flow rate equation 3.4 becomes,

$$\dot{V} = \frac{\dot{m}}{\rho} \qquad \textbf{3.4}$$

After plugging all the known values into equation 3.4, the required mass flow rate required to remove a heat flux of 1000 W/cm^2 is greater than or equal to 0.3289 l/min

(0.0869 GPM). The required pressure head was determined from below. A complete solution is provided in Appendix: A.

After interpolating the absolute pressure is:

$$P_{absolute@34°C} = 1.004 Bars = 0.1004 MPa \ (14.56\, psi)$$

According to the calculations above, the required pressure drop was estimated to be $\cong 0.207 MPa \ (30\, psi)$. Therefore, by using the parameters in Table 3.4 and using McMaster as the supplier, a desired pump was selected to meet the needs of the expected pressure drop in the loop.

Table 3.4. Pump selection decision matrix

Criteria Percentage	Pressure 20%	Temperature 20%	Flow Rate 20%	Two-Phase 40%	Total
Gear Pump					
McMaster Carr # 4272K	5	4	4	2	3.4
McMaster Carr # 43095K w/ Packing Seal	5	5	1	2	3
McMaster Carr # 43095K w/ PTFE Seal	5	4	3	2	3.2
Rotary Pump					
McMaster Carr # 8074K	5	3	4	2	3.2
Grainger # 1P610	5	4	4	3	3.8

Table 3.4 shows the decision matrix taken to select the pump for the system. Each criterion in the table is given a percentage based on its importance in the function of the overall loop. The criterion was selected based on what was deemed important in view

of the types of phase excepted in the loop. Once the weights were applied to the criteria each component was weighed on a scale of 1 to 5. A category of how the pump could handle two phase flow was included because a vapor phase was anticipated in the loop. After each component was weighed a total was taken and the one with the highest overall total was selected.

Initially, a 372.85 W (1/2 hp) gear pump with a mass flow rate of 8.33 l/min (2.2 gpm) was selected. However, after further research, it was determined that a gear pump was not suited for flowing two-phases. Based on this information, a more suitable alternative turned out to be a rotary pump. After determining that a rotary pump was most suited to this task, Grainger Industrial Supply was selected as the supplier and the rotary pump shown in Figure 3.9 was selected. The pump has mass flow rate of 18.92 l/min (5 gpm) at a zero pressure head and a maximum pressure of 0.2758 MPa (40 psi).

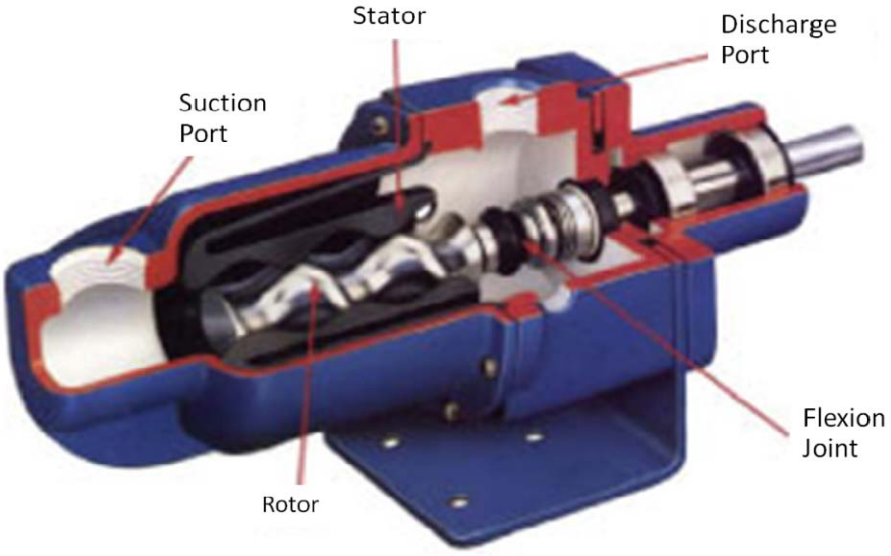

Figure 3.9. MOYNO 2.2 gpm pump cut-away

Given that the maximum speed of the pump is 1750 RPM, a motor capable of operating at the same speed was selected to power the pump. Since the pump was purchased from Grainger, they were also selected as the vendors for the motor. The pump selected was a 124.28W (1/6 hp) permanent magnet DC motor in Figure 3.10(a) with a maximum speed of 1800 RPM that had a speed controller shown in Figure 3.10(b).

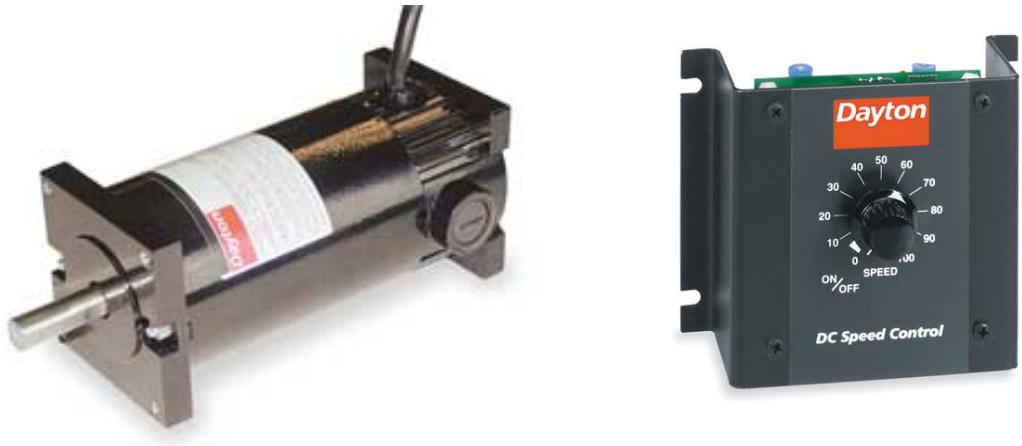

(a) **(b)**

Figure 3.10. (a) Dayton DC motor (b) Dayton variable speed controller

In view of the fact that the variable speed controller has no direct relationship between its speed readings and the actual speed of the motor, a crude tachometer was developed using an on/off proximity probe. The probe is setup up such that as the motor rotates, it turns the sensor to "ON" or "OFF" position. The shaft of the motor has a flat side, which is out of proximity to the probe as depicted in Figure 3.11 (a) thus the "OFF" position. On the other hand, the curved side is in proximity to the probe as depicted in Figure 3.11(b)) thus the ON position.

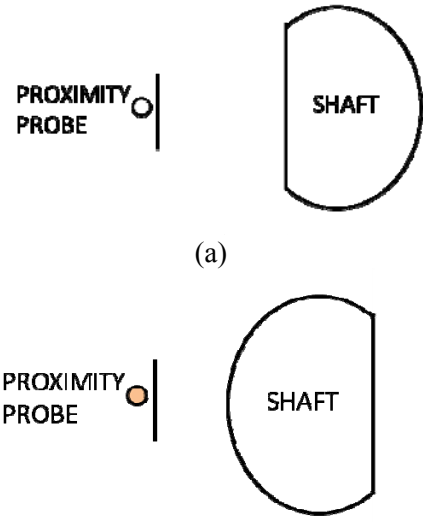

Figure 3.11. (a) Proximity probe off when it is on flat side of shaft, (b) Proximity probe on when it is on a curved portion of the shaft

When a known voltage is applied to the probe, then the voltage output would be approximately the same as the known input the probe is OFF. When the voltage is less than the input, then the probe is ON. By measuring the time period between the "ON" and "OFF," the speed of the motor can be determined.

Figure 3.12 shows the potential step wave created by the proximity probe when the shaft rotates in and out of the range of the probe. The start and end of the period are shown as dashed lines and the voltage across the proximity probe is the bold solid line. The speed or rotation in RPM can be determined from the 60 divide by the period of the voltage wave. The proximity probe uses the capacitance methods to sense the presence of an object interfering with its electric field.

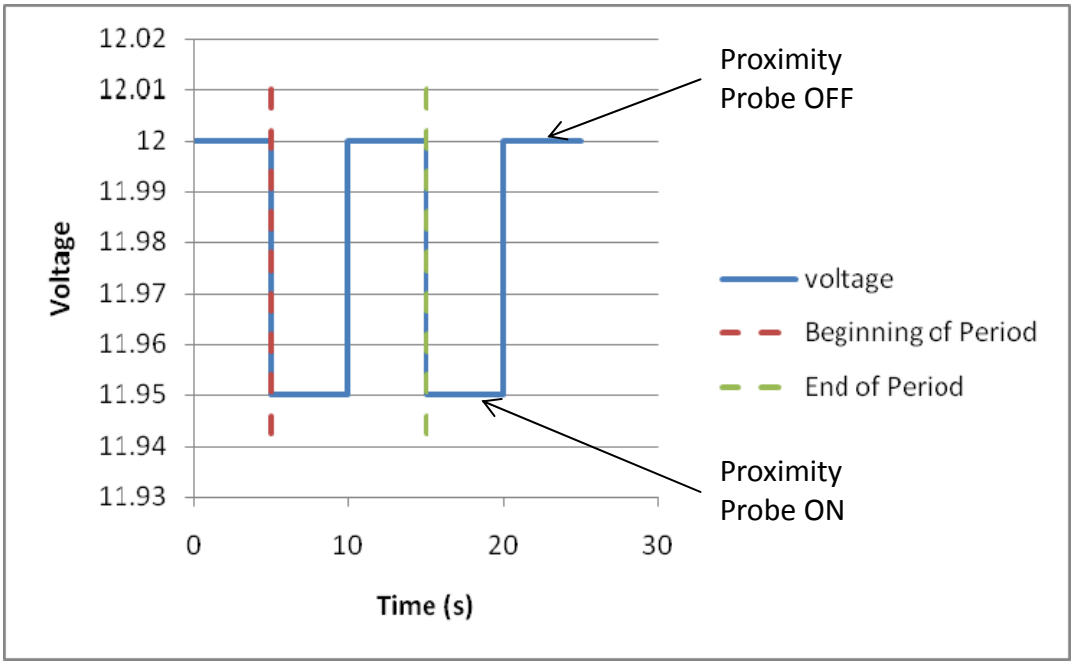

Figure 3.12. Potential output of proximity probe when exposed to a 12 Volt input

3.1.7 Phase Separators

It is sometimes necessary to separate the phases into their single phase components when dealing with two-phase flows. One reason for the need to separate the fluids is that it is undesirable for two phases to coexist at certain parts of the system. However, it is possible that there would be some vapor left when the vapor condenses back to its liquid state. Therefore, the use of components such as ejectors, centrifuges, cyclones, and filters could be very helpful in separating the two-phases before they enter the pump. This further increases the pumping load and stability requirements for circulating two-phase flow. Separating the phases does not always have to have a

negative effect in a cooling system. It can also be beneficial in a system where the vapor could be used to atomize the working fluid in the nozzle. The alternative would be to use air, thus requiring the need for an external air compressor.

The purpose of the cyclone is to separate the liquid phase from the vapor phase so that the vapor phase can be used to atomize the liquid phase. The cyclone was selected as a phase separation system because it can be used without external power or moving parts. A cyclone design was developed to separate the two-phase flow into its individual liquid and vapor components as depicted in Figure 3.13(a). The fluid that enters the cyclone is tangentially pumped from the rotary pump. In the cyclone, the force exerted by the centrifugal motion (Figure 3.13(b)) of the fluid forces the heavier fluid toward the walls and the denser vapor toward the center.

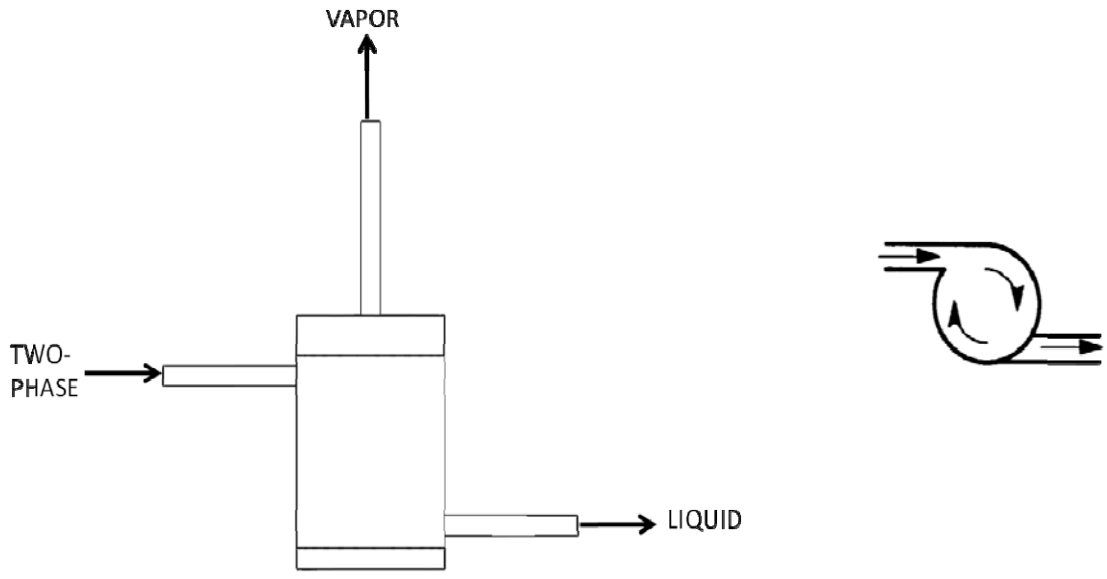

(a) (b)

Figure 3.13. (a) Cyclone showing individual phase exits, (b) Image of how flow enters tangentially and is forced radially

As the heavier fluid is forced against the walls, it travels down the exit in the bottom of the chamber, while the denser vapor exits through the top due to its buoyancy. The system uses an atomized spray to reduce the overall heat flux. The two-phases are mixed just before the nozzle exit. Atomizing of the flow breaks-up the injected fluid into smaller droplets to aid in the vaporization of the fluid upon impingement onto the heated surface.

Figure 3.14 shows the different designs of the cyclone throughout the development process. All three designs are similar, but the only modification was the location of the liquid outlet. The reason for changing the location of the outlet was to allow ease of manufacturability and installation.

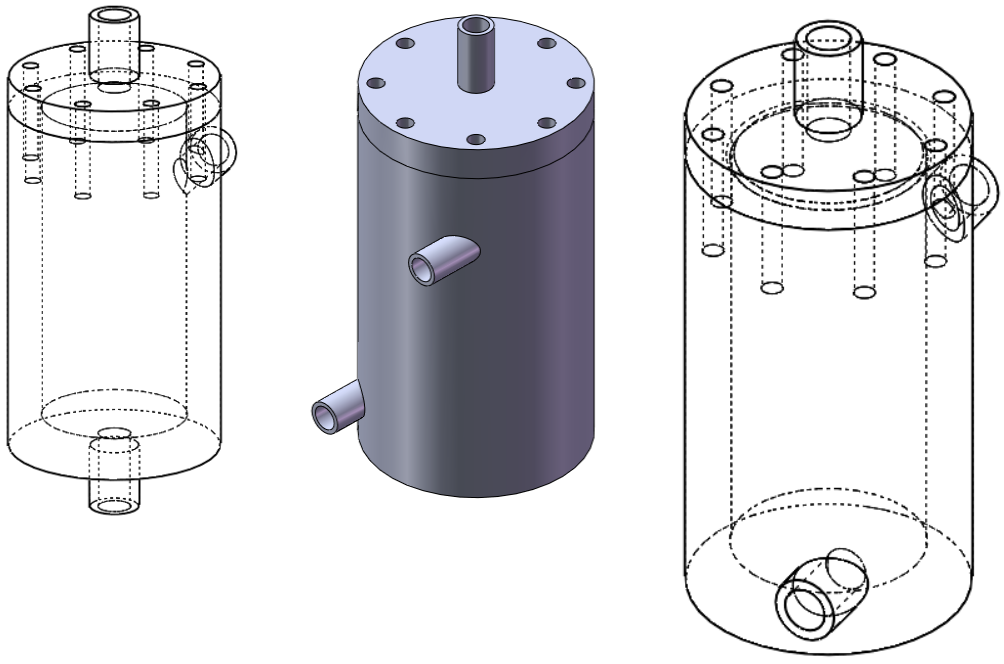

(a) (b) (c)

Figure 3.14. (a) Initial cyclone design, (b) Modified cyclone design, and (c) Final cyclone design

As a result, from the initial design in Figure 3.14(a) to the modified design in Figure 3.14(b), the outlet is moved from the bottom to the side. By moving the outlet to the side, the design allowed for the bottom of the cyclone to be used as a stable base to mount the system without the use of supports. From the modified design to the final design in Figure 3.14(c), the outlet is rotated 180 degrees around the cylinder. This modification allowed the cyclone to be located in close proximity to the mounting board. It also allowed the piping connecting the components to have a straight entrance and exit from the cyclone.

Other small modifications to the final design were made from an ease of manufacturability perspective. One modification was to create a flange at the bottom as shown in Figure 3.15(a), making the center section a simple bored out part. To aid the fluid drainage process, a conical shape was added to the bottom flange to deter any fluid from stagnating in the bottom of the cyclone. The chamfered section on the top flange depicted in Figure 3.15(b) was included to aid direct flow of vapor to exit of the cyclone.

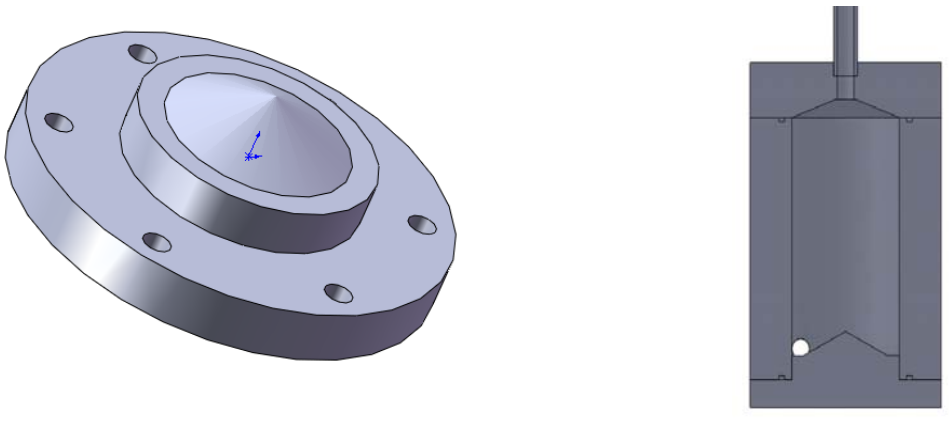

(a) (b)

Figure 3.15. (a) Bottom flange of cyclone, (b) Section view of Cyclone

Another modification made was the addition of gaskets to make sure that the system did not leak. To check the functioning of the final design, a fluid analysis was performed with commercial CFD software called Fluent to visualize the fluid flow around the chamber. After the analysis was complete, the next step was to select a construction material. The material selected was stainless steel due to its strength and corrosion resistance.

3.1.8 Heat Exchanger

The selection of the heat exchanger began with the determination of the heat load that needed to be removed from the working fluid. The example given below assumed a temperature drop of the chiller fluid by 10 °C. The process is illustrated in Figure 3.16. The loop heat exchanger interacted with a refrigeration cycle using R134a to dump the heat to the room environment thus creating a cold temperature heat sink. The refrigeration chiller was capable of achieving lower temperatures when mixtures of ethylene glycol and water were used.

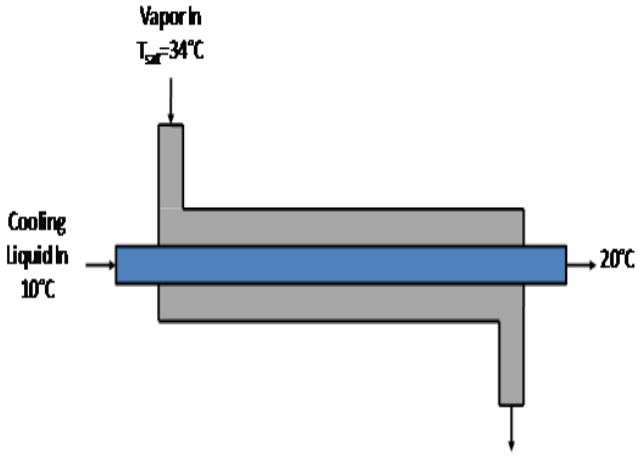

Figure 3.16. Heat exchanger schematic

From the calculations performed, the required removal rate was 1,674.5 W (5,715 But/hr) for the heat exchanger, and the maximum flow rate was 2.396 l/min (0.6329 GPM). These numbers assume Novec-7000 is the working fluid in the loop and water is the working fluid in the chiller. A complete solution is provided in Appendix B. Now that the necessary parameters were known, the criteria were developed. From these and other pertinent parameters presented in Table 3.5, a selection criterion was developed to procure the heat exchanger.

Table 3.5. Heat exchanger decision matrix

Criteria Percentage	Cooling Capacity 20%	Flow Rate 20%	Temperature 20%	Pressure 20%	Size 20%	Total
McMaster Carr # 34965K	1	1	5	5	3	3
McMaster Carr # 3586K	2	5	5	5	1	3.6
McMaster Carr # 8507T	5	4	5	5	5	4.8
McMaster Carr # 8601T	3	5	5	5	5	4.6

From decision matrix in Table 3.5, it was determined that a shell-and-tube heat exchanger was the best match. Two heat exchangers were used to meet the heat removal requirements. In the present setup, a cross flow arrangement was used with two 1,318.5 W (4500 Btu/hr) heat exchangers in series and a 2.635 kWh (9000 BTU) chiller capable of removing 5kW of heat. The chiller was purchase as an off-the-shelf (OTS) item from McMaster Carr. The chiller allowed the use of ethylene glycol and/or water mixture as

the working fluid. The water - ethylene glycol mixtures can access temperatures lower than -30°C.

3.1.9 Vacuum Pump

Proper selection of the vacuum pump was necessary to facilitate the removal of incondensable fluids (air) from the chamber environment, because incondensable fluids hinder the heat removal capabilities of the fluid, and allows heat to be transported from the heater into the environment via the chamber walls. Creating a vacuum in the chamber also allows the working fluid to boil at a lower temperature, therefore, increasing performance of the system. The performance of the system is related to the difference between the maximum and minimum temperatures. Equation 3.5 is used to determine the required vacuum pump size. (http://www.graco.com)

$$S = \frac{\forbar{V} \times F}{t} \qquad \textbf{3.5}$$

Where,

S = Pump Size (CFM)
$\forbar{V}$ = Total Volume (ft^3)
F = 1 for vacuum up to 15 in-Hg
2 for 15<vacuum ≤ 22.5 in-Hg
3 for 22.5<vacuum ≤ 26 in-Hg
t = Required Time (minutes)

The volume of the individual components in the loop can be calculated as,

$$Volume_{Piping} = 370(lenght) \times 0.1075(area) \cong 40\ in^3$$

$$Volume_{Cyclone} \cong 19\ in^3$$

$$Volume_{Accumulator} \cong 181\ in^3$$

$$Volume_{Heat\ Exchanger} \cong 28\ in^3$$

$$Volume_{Injector\ \text{Chamber}} \cong 141\ in^3$$

After determining the component volumes, the total volume was calculated as,

$$Volume_{Total} \cong 400\ in^3 = 0.2315\ ft^3$$

Using a desired time of 10 minutes and a desired pressure of 16 in-Hg (15.13 kPa), which means the correction factor F = 2. The required pump size in 5 in-Hg increments is: $S = 0.0463\ CFM$.

For a 16 in-Hg the pump size, the S is multiplied by 16/5, to give S = 0.1482CFM.

Working backwards using data for a pump from McMaster Carr Catalog shown in Figure 3.17 the pump time can be determined. The pump was capable of 1.1 CFM needs the following time elapse. To calculate the time required to achieve 16 in-Hg, use Equation 3.6 as:

$$t = \frac{\cancel{V} \times F}{S} \qquad \textbf{3.6}$$

Figure 3.17. Gast vacuum pump

Plugging in the new numbers, the required time in 5 in-Hg increments is,

$$t = \frac{(0.2315)(2)}{1.1} = 0.421\,\text{min}$$

So the total time is 1.35 minutes. The time was found sufficient to remove the incondensable gases before system initiation.

3.1.10 Heater/Injector Chamber

The injector chamber was developed based on the performance described by the maximum temperature, pressure, and heat flux tolerated by the design requirements. The initial design consisted of a 5"diameter x 3" long 316 stainless steel billet that was machined with a 2.5" diameter hole 2" deep with a chamfered edge toward the top to direct the vapor from the impingement surface upward through the vapor outlet as illustrated in Figure 3.18.

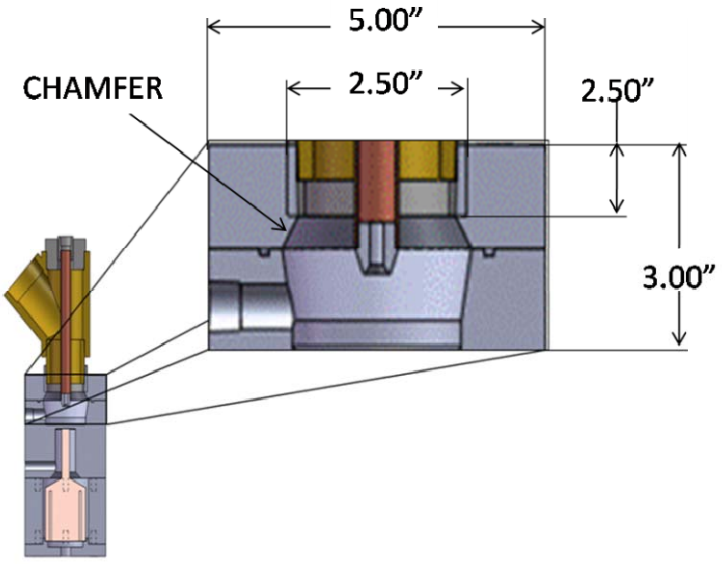

Figure 3.18. Section view of original heater/injector chamber with blowup of injector chamber

From preliminary experiments, the need to refine the initial design was necessitated by the following disadvantages. The disadvantages of the original heater/injector chamber system were:

1. The inability to visualize the spray impingement process
2. The chamber did not have fluid drainage making the process restart time consuming, because of the need to wait for the fluid to boil off in the event that the chamber flooded
3. The distance between the liquid vapor mixing for atomization and the actual exiting of the nozzle was excessive
4. The overall accessibility of the system was limited

A redesign was proposed to mitigate the aforementioned disadvantages. To resolve the first issue, a multitude of methods were explored to determine a way of incorporating flow visualization into the original injector chamber design. Originally, one of the tasks was to determine whether or not the chamber would flood. One of the proposed methods for determining flooding was to install a capacitance probe in the chamber so that if the liquid level began to increase the voltage would change thus allowing an indirect method of the presence of liquid pool in the chamber. The capacitance gauging method was deemed impractical, after an individual component test determined that the capacitance probe was an on/off probe with limited resolution to infer liquid depth. The second method was to install a sight glass to the chamber. This option was discarded because the optimal location had to be tangential to the heated surface, hence sight installation would be difficult. Therefore, it was proposed that a new design be considered. The new chamber was designed and implemented based on the illustrations in a CAD design shown in Figure 3.19. The success of the new design was

based on new philosophy that instead of manufacturing everything from scratch, the bulk of the components would be purchased off-the-shelf making the assembly of the chamber relatively easy. The new design would also allow for the addition of a vacuum system to the entire loop. The addition of the vacuum system would mean that the new chamber had to be fully sealed in order to maintain a vacuum.

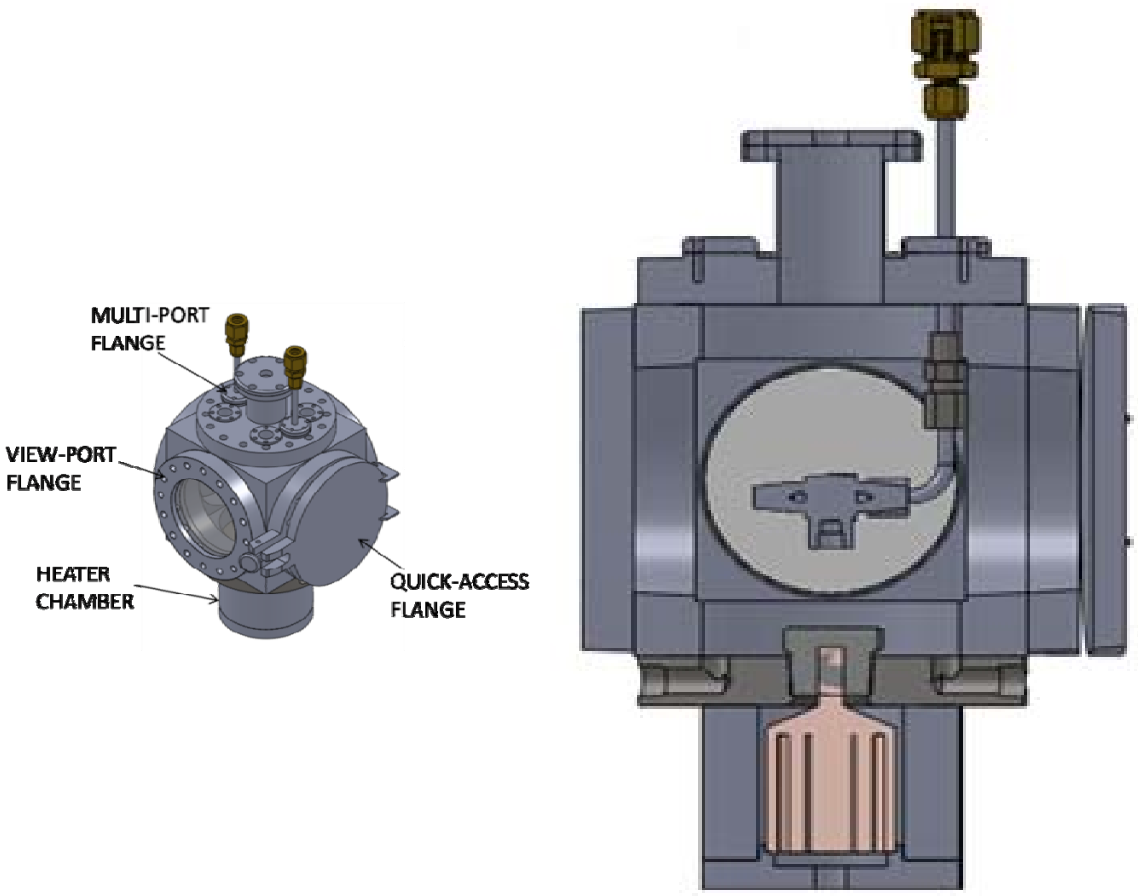

(a) (b)

Figure 3.19. (a) New heater/injector chamber, (b) Section view along drainage holes

The new design consists of components selected and purchased from MDC-Vacuum. The use of the vendor parts allowed all of the aforementioned disadvantages to be resolved. All of the components were connected to a 0.1524 by 0.1524 meter cube (6 by 6 inch). Given below is an itemized list of the resolved issues:

1. To aid in flow visualization, two view ports with a 0.0889 m (3.5") diameter view area were added.

2. To aid in chamber drainage, a custom flange with two drain holes, on opposite sides of the heated plug (illustrated in Figure 3.20) was created.

3. To have the fluid remix directly before being ejected from the nozzle, the liquid and vapor line were kept separate until they reached the tee-fitting holding the nozzle.

4. To make sure that the nozzle and heated surface where accessible, a quick access flange was installed.

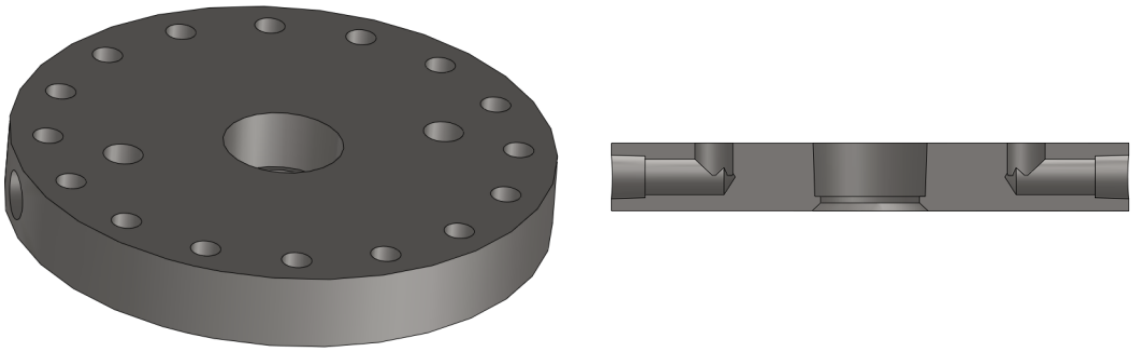

(a) (b)

Figure 3.20. (a) Custom drainage flange (b) Transparent image of drainage flange

After the first injector chamber disadvantages were resolved, the new issues that arose when the old heater was incorporated into the new design had to be also resolved.

Originally in the design process of the new chamber, it was decided that a hollow stainless steel threaded nipple would be used as shown in Figure 3.21(a). Plug would be used to transfer the heat from the copper block to the sealed injector chamber. Plug design was chosen because of the ease of heater changeability. After determining that the heat transfer would be more efficient if the impinging liquid was in direct contact with the heated surface, an extension block was made as shown in Figure 3.21(b).

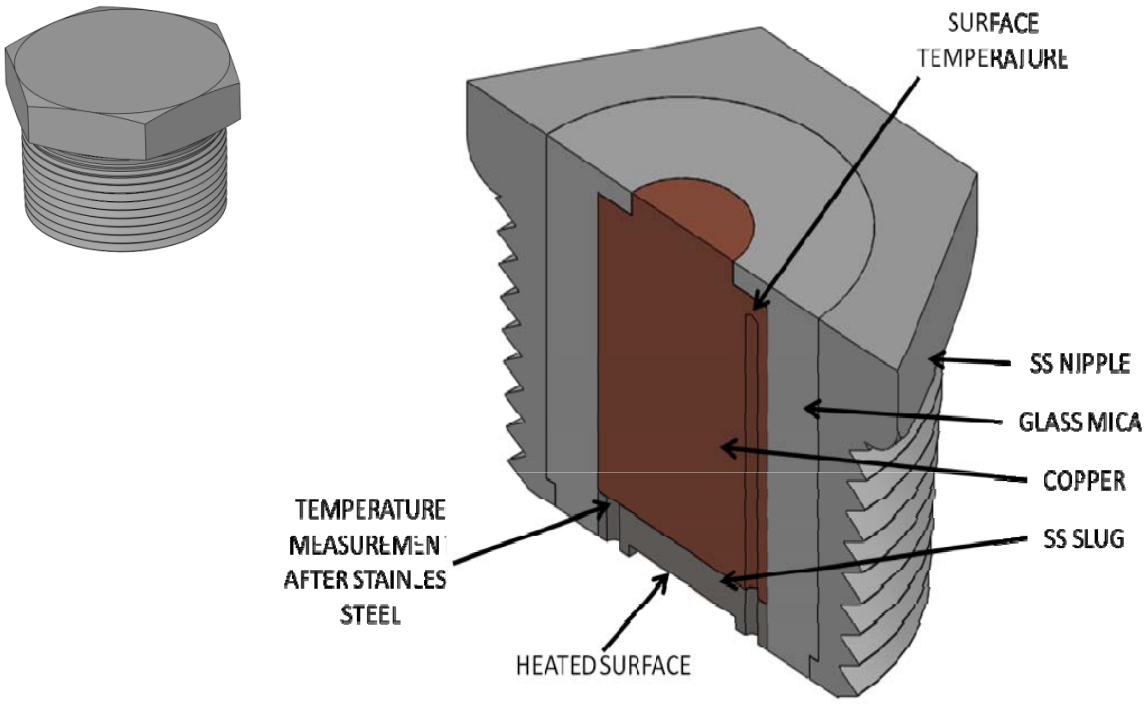

(a) (b)

Figure 3.21. (a) Hollow stainless steel plug, (b) Section view of the extension block shown in (a)

The extension block was a stainless steel nipple with a glass mica slug insert. The glass mica was used as a thermal insulator to reduce the amount of radial heat lost from

the copper block to the chamber walls. Glass mica can withstand a maximum temperature of 800 °C. A copper plug was press fitted into the glass mica and the assembly was capped with a stainless 0.375 cm (0.125") long steel plug. Press fit calculations were done to determine proper interference between materials. The induced internal stresses were necessary to withstand the fluid pressure, but not excessive enough to cause the glass mica to fracture. The extension plug incorporated three temperature measurement locations. One location was 0.3175 cm (0.125") distance from the heated surface. This location was classified as the surface temperature measurement level. Then another hole was drilled at the bottom of the copper slug to measure the temperature at the top of the stainless steel plug. The third temperature measurement was taken at the bottom of the stainless steel plug. So the heat flux was measured across the stainless steel plug and the heat flux was related to the supplied heat flux based on the power supply settings. The supplied heat flux was related to the surface temperature.

The heater chamber shown in Figure 3.22 was designed with the above design requirements parameters (i.e. maximum temperature, pressure, and heat flux). The main focus of the heater chamber was to ensure that the energy that was being supplied reached the heating surface. During the running of experiments, it was determined that there was a large amount of heat loss from the heater to the surrounding chamber. The most likely cause of the heat loss was due to natural convection and radiation heat transport modes. Efforts were made to excessively apply insulation to the chamber to limit the heat loss to the environment.

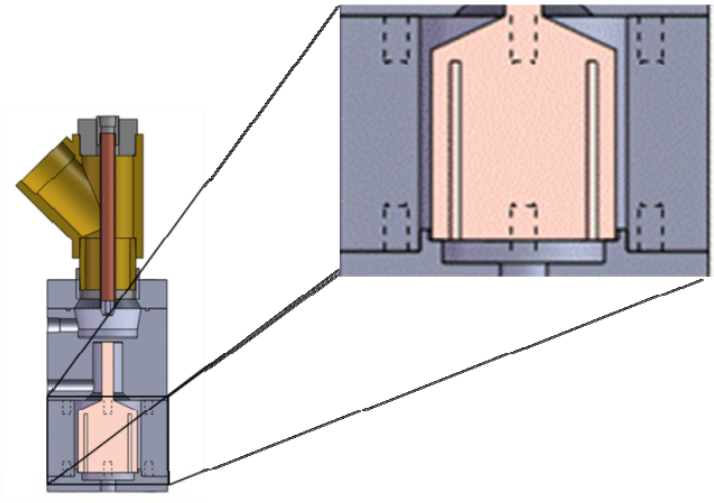

Figure 3.22. Section view of heater/injector chamber with blowup of heater chamber

Like the injector chamber describe above, a redesign of the chamber was needed to further decrease the thermal loses between the heater and the chamber walls. Therefore, a new system using the aforementioned design philosophy was developed, which required the use of components from MDC-Vacuum. To reduce heat losses due to natural convection transport mode, a vacuum chamber depicted in Figure 3.23 was developed.

To reduce heat losses due to the radiation transport mode, a reflective material was inserted between the stainless steel wall and the copper block thereby reflecting the majority of the heat back to the source. To determine an effective reflective material to calculate the amount of energy emitted, the equation below was used.

$$\dot{Q}_{emitted} = \varepsilon \sigma A_s T_s^4 \qquad \textbf{3.7}$$

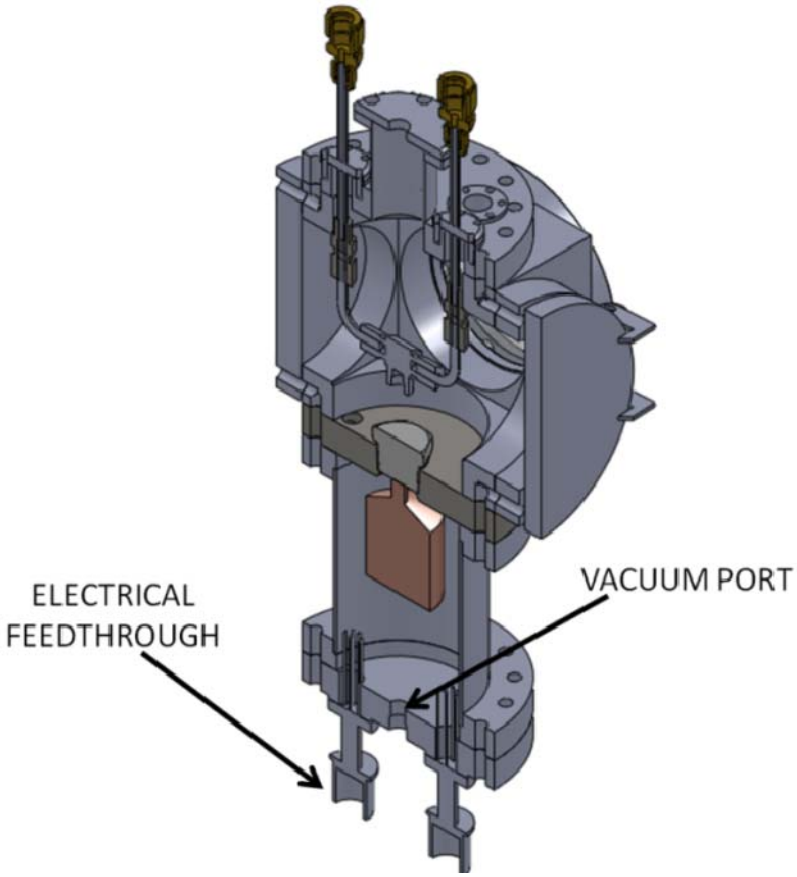

Figure 3.23. Heater/Injector chamber with vacuumed heater section

Thus, after plugging in the emissivity for copper and assuming a surface temperature of 800 °C, it was determined that the copper block would emit 25.186 W of energy. Given that the amount of energy emitted was known, it was possible to determine the amount of energy that could be reflected back to the block. Radiation energy exchange can be determined by the amount of energy that a specific material might absorb (see equation 3.8).

$$\dot{Q}_{absorbed} = \alpha \dot{Q}_{emitted} \quad \textbf{3.8}$$

Equation 3.8 and values from Table 3.6 were used to determine the most efficient reflective material.

Table 3.6. Radiation absorbance table of specific materials

Material	α	$\dot{Q}_{absorbed@800°C}\ (W)$
Dull Stainless Steel	0.50	12.593
Polished Stainless Steel	0.37	9.318
Polished Aluminum	0.09	2.267
White Paint	0.14	3.526

Radiation absorbance values in Table 3.6 indicate that the material that absorbs the least amount of energy is polished aluminum. For example, a heater block emitting 25.186 Watts in the form of radiation heat to the polished aluminum lining would only absorb 2.267 Watts of energy and would reflect 22.919 Watts back to the block.

3.2 Experimental Setup

The following section is devoted outlining a step by step procedure necessary to assemble the thermal loop.

A. Built wood structure as shown in Figure 3.24:
   i. Obtained components
      1. 2x4 wood
      2. Plywood
      3. Nails

4. Screws

5. Nuts and Bolts

6. Metal supports

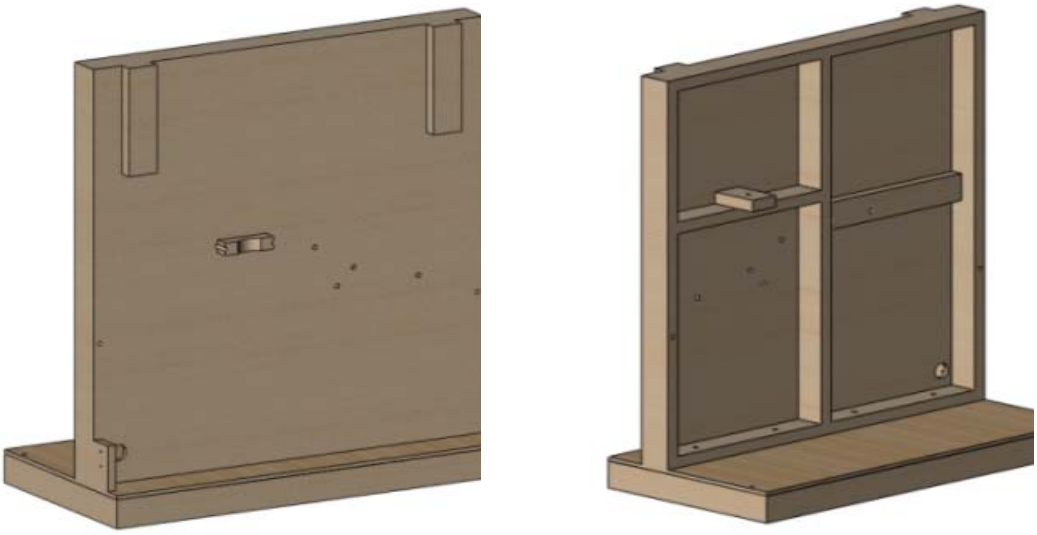

(a) (b)

Figure 3.24. (a) Front view of wooden board structure (b) Back view of wooden board structure

ii. Assembled the wood support structure:

1. Constructed the top structure with the 2x4 boards, and then applied the plywood sheeting

2. Constructed the base of the structure in a similar manner

3. Placed the top structure on the base and drilled holes to allow fastening with the bolts

4. Drilled holes on each side of the top and bottom board to add metal supports

5. Nailed two boards to the top structure to offset the heat exchangers

6. Cut a cylindrical hole in a 2X4 to serve as a cradle for the cyclone

B. Added components to structure as shown in Figure 3.25:

i. Pump

ii. Heat exchangers

iii. Cyclone

iv. Heater/Injector chamber

v. Accumulator

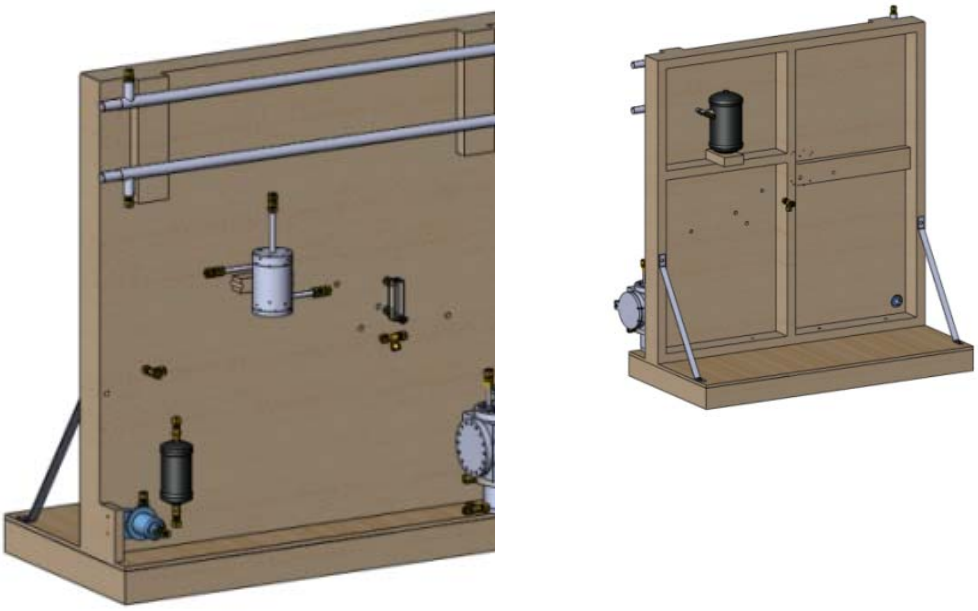

(a) (b)

Figure 3.25. (a) Front view of board with components, (b) Back view of board with components

C. Connected components with compression fittings and copper tubing as shown in Figure 3.26

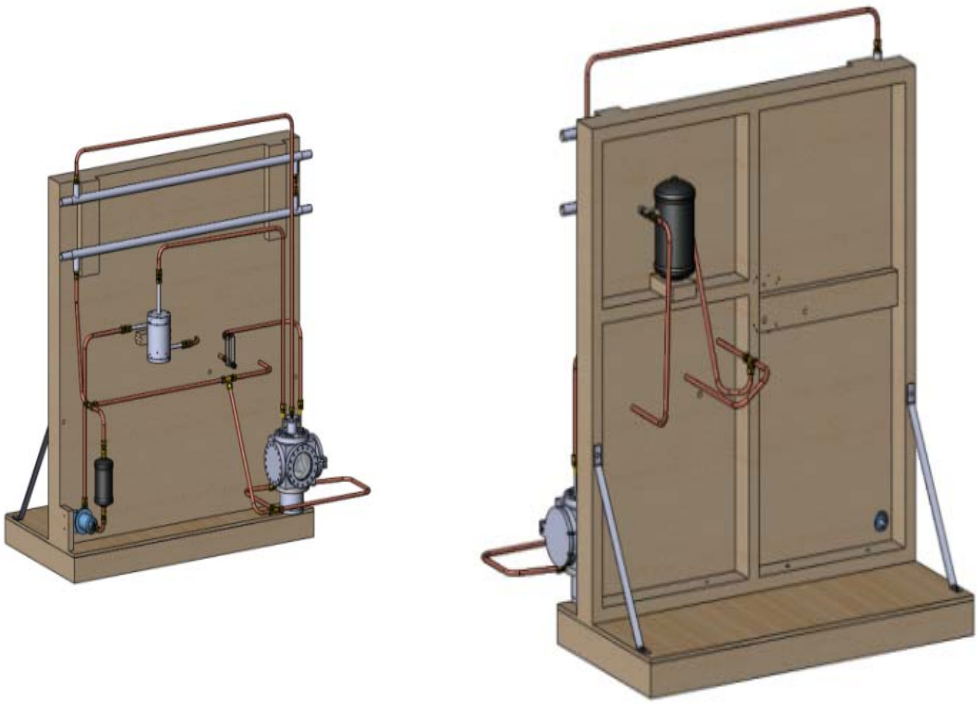

(a) (b)

Figure 3.26. (a) Front view of structure with all components and tubing, (b) Back view of board with all components and tubing

3.3 Test Procedure

3.3.1 Individual Component Test Procedures

Before assembly of the loop could begin, the individual components had to be tested for functionality and initial baseline performance. The following section will describe the procedures that were taken to test the individual components. All tests were performed on an open loop system.

Pump Test Procedures

A. Parameters that were tested:

i. Flow rate (m^3/s), speed (rpm)

ii. Differential pressure

iii. Pump efficiency (head loss)

B. General procedure:

i. Set Pump speed

ii. Primed the pump

iii. Checked inlet pressure, flow rate, and temperature

iv. Checked the outlet pressure, flow rate, and temperature

C. Step-by-step test procedure as illustrated by Figure 3.27:

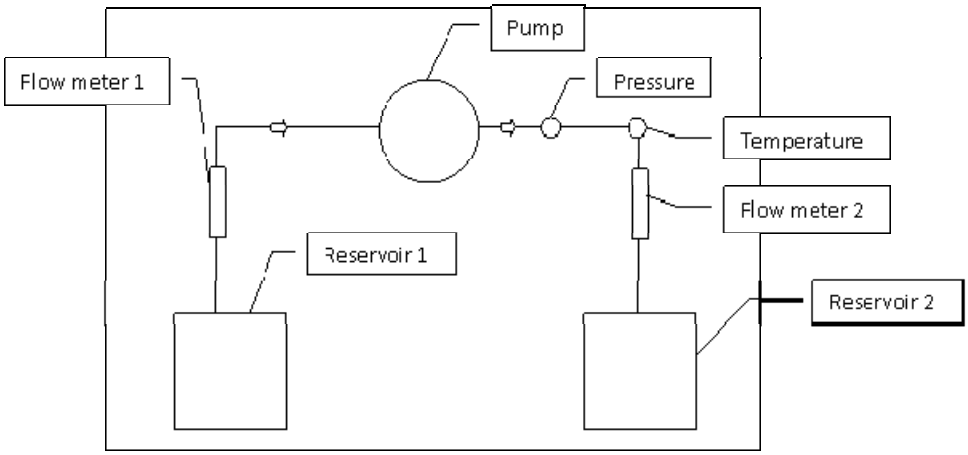

Figure 3.27. Pump test component layout

i. Made all initial component connections:

1. Intake flow meter

2. Outlet pressure gauge, flow meter, and temperature gauges

3. Inlet and outlet reservoir connections

ii. Half filled both reservoirs with water

iii. Set pressure initial as the atmospheric pressure

iv. Measured the temperature of intake reservoir water

v. Primed the pump

vi. Determined the changes in the outlet pressure, temperature, and flow rate based on the pump speed

vii. Calculated pump efficiency

Motor Test Procedures

Connect the motor as depicted in Figure 3.28 and check to see if variable speed controller works.

Figure 3.28. Actual pump test setup

Injector Test Procedures

A. Parameters that were tested:

   i. Determined effective pressure

   ii. Determined the amount of liquid over a set time

   iii. Velocity

   iv. Flow rate

   v. Determined the spray pattern

   vi. Spray area

   vii. Impact force

B. General procedure:

   i. Used previous pump set-up

   ii. Determined differences in cone nozzle spray pattern with pump speed

   iii. Determined pressure effect in contact area

C. Step-by-step testing procedures as illustrated in Figure 3.29 along with actual testing layout in Figure 3.30:

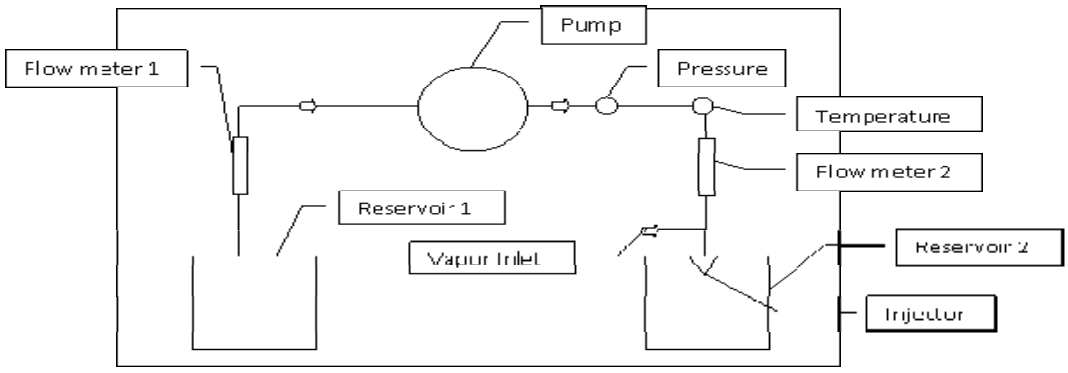

Figure 3.29. Injector test component layout

i. Installed T-fitting for compressed air hook-up

ii. Set time laps camera

iii. Connected injector to outlet of pump set-up

iv. Began experimentation

v. Data that was collected. The following parameters were determined:

1. The effective compressed air to input into system
2. The spray area using grid sheet
3. The effect of pressure on spray pattern
4. The effective distance
5. The amount of liquid dispersed over set time
6. The flow rate
7. The velocity
8. The impact force
9. The discharge pressure
10. The effect of pressure on spray area

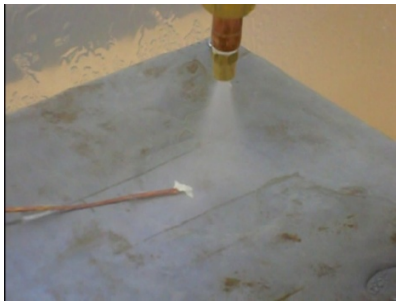

Figure 3.30. Actual injector test

vi. Repeated steps 3-5 for other injectors

vii. Ended testing

Heater Cartridges

A. Parameters that were tested:

i. Heat flux

ii. Temperature based on voltage

B. Step-by-step test procedure illustrated in Figure 3.31:

i. Cemented thermocouple to heater cartridge

ii. Connected thermocouple to data acquisition

iii. Connected heater cartridge to DC power supply

iv. Determined heat flux

v. Determined temperature based on voltage

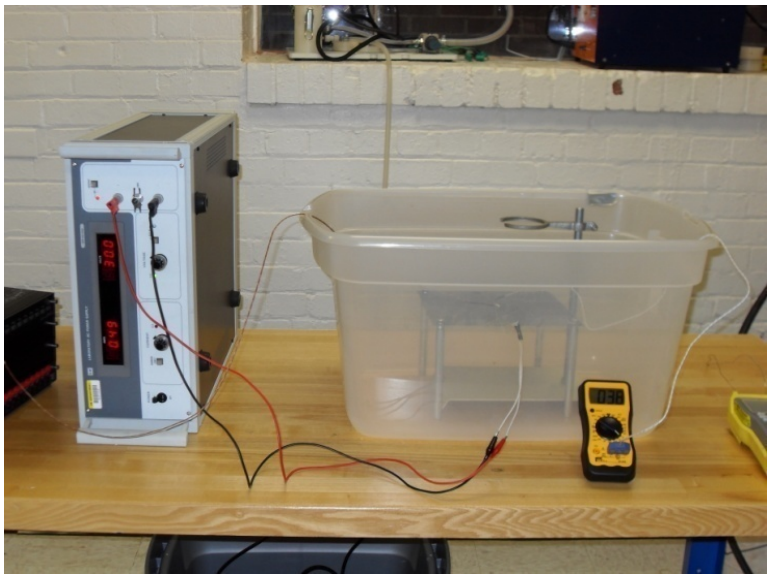

Figure 3.31. Actual heater cartridge test

Heat exchanger test procedures while connected to chiller

A. Parameters that were tested:

   i. Chiller flow rate

   ii. Inlet and outlet temperature for chiller

   iii. Inlet and outlet temperature for steam

B. Step-by-step procedure as illustrated in Figure 3.32 along with actual testing layout in Figure 3.33:

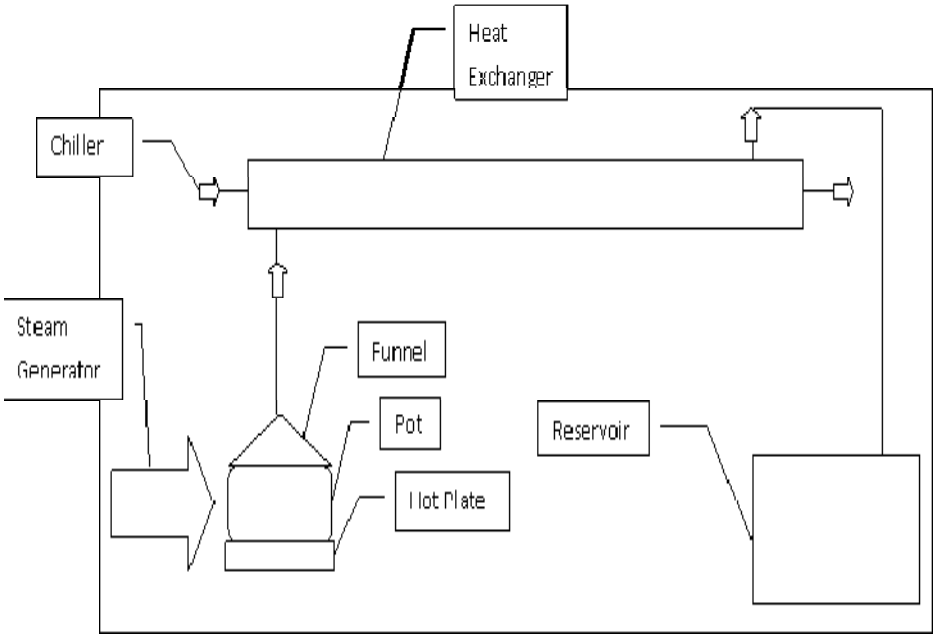

Figure 3.32. Heat exchanger component layout

   i. Created a steam generator

      1. Hot plate

      2. Pot filled with water

      3. Connect hose

ii. Connected chiller to HX

iii. Connected steam generator to HX

iv. Connected instrumentation

v. Determined effective flow rate of chiller to get maximum chilling

vi. Determined the outlet temperature of converted vapor

vii. Determined the amount of liquid in the reservoir compared to the initial amount of liquid in steam generator

Figure 3.33. Actual heat exchanger and chiller test

Heating Chamber Test Procedure

A. Parameters that were tested:

i. Rate of vaporization

ii. Overall external temperature

iii. Internal temperature

iv. Injector interface with heater

B. Step-by-step test procedures:

i. Installed all heater cartridges in heater

ii. Installed heater in container

iii. Measured temp at contact spot

iv. Measured internal and external temperatures of chamber

v. Determined how each injector interacts with the chamber at different pressures and speeds

Cyclone Test Procedures

A. Parameters that were tested:

i. Inlet and outlet flow rate

ii. Inlet and outlet pressure

B. Step-by-step test procedures illustrated in Figure 3.34:

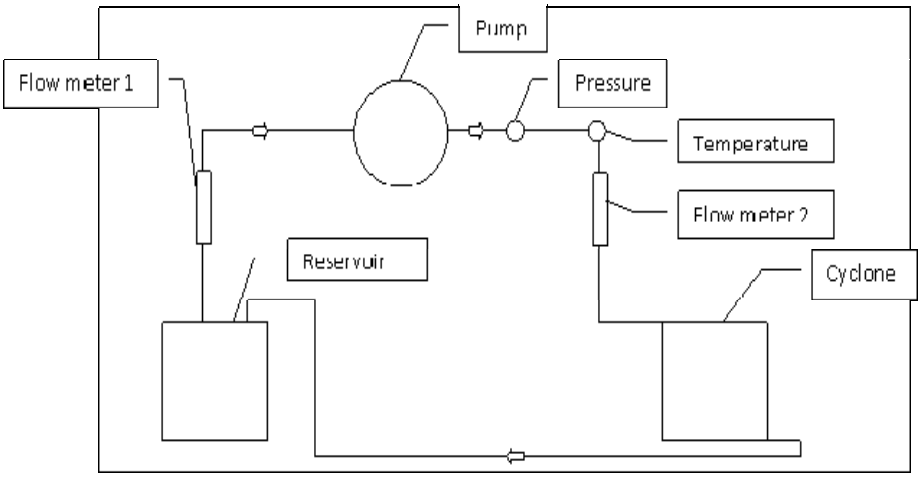

Figure 3.34. Cyclone test component layout flow chart

i. Connected pump system to cyclone

ii. Connected instrumentation (Pressure gauge, and flow meter)

iii. Determined effective flow rate to get appropriate cyclone shape

3.3.2 Loop Setup and Shutdown Procedures

Initial Thermal Loop Setup

1. Connected a vacuum pump to the inlet of the rotary pump to create a negative pressure in the system

2. Opened the three-way valve located before the pump and turn the vacuum pump on

3. Closed the three way valve and turn the pump off

4. Closed the three-way valve on the inlet line of the injector chamber, the flow meter, and closed the needle valve at the exit of the heat exchanger, and the three-way valve at the inlet of the pump

5. Disconnected the vacuum pump and connected a hose submerged in a jug of water

6. Opened the three-way valve and the negative pressure in the system will pull fluid from the jug into the chamber. (NOTE: A small portion of this will be air)

7. Once the fluid in the system began to fill up in the injector chamber, closed the three-way valve to stop the fluid. Placed the submersible in a bucket full of the working fluid

8. The system was now ready to be run if air was desired in the system

9. The vacuum pump was connected to the quick release valve on the vapor inlet line to remove the air from the system

10. Turned the pump on and opened the valve to remove air from the system

11. When the liquid stopped flowing through the pump the valve was closed and the pump was shut off

Testing Setup

1. Connected thermocouples and pressure transducers to data acquisition systems (DAS)
2. Turned DAS on
3. Turned the computer on and connected to DAS
4. Setup DAS
5. Connected the cartridge heaters to the DC power supply
6. Set DC power supply to 63 Volts and set the current limit to the maximum amperage
7. Turned DC power supply ON to heat heaters to steady-state
8. Opened all three-way valves
9. Opened flow meter all the way
10. Started the pump
11. Began the data collection

Shutdown Procedure

1. Turned off the heater
2. Closed accumulator needle valve
3. Closed vapor three-way valve
4. Closed flow meter
5. Waited till no liquid was left in injector chamber then closed the drain three-way valve
6. Immediately turned the pump off

Emergency Shutdown Procedure

1. Turned DC power supply off

2. Turned Pump off
3. Closed all valves
    a. Liquid flow meter valve
    b. Vapor valve
    c. Accumulator valve
    d. Drainage valve

3.3.3 Test Matrix

Test matrixes were developed for each individual component such that determination of whether a component could be deemed successful while operating in the thermal loop.

The objective of the heater characterization was to develop a heating curve for the maximum heat flux while the loop was operating from a minimum to maximum flow rate. The reason for determining maximum heat flux at minimum and maximum flow rate was to bracket the data. The process of determining this is listed below.

1. Started the pump at the lowest flow rate ($\dot{m}$)
2. Started the voltage to the heater at 63 volts
3. Calculated the ($\dot{Q}$) by multiplying the voltage by the current displayed on the dc power supply
4. Calculated heat flux ($\dot{q}$ W/m^2) by dividing the energy by heater surface area
5. Ran the heater until steady state temperature was reached
6. Plotted $T_{surface}$ (°C) vs. time
7. Repeated steps 2 – 7 at the maximum flow rate after the heater has cooled back down to room temperature

The objective of this section is to determine if two phases could be separated after entering the cyclone. To determine the extent of phase separation, a relationship between pressure and mass flow rate was derived. The relationship required that the pressures at the points indicated in Figure 3.35 be measured. Secondly, the relationship required that the densities of the liquid and vapor fluids were known. It also required that at least one mass flow rate was known. The following procedure used to determine the separation success:

1. Used void fraction sensor to determine the quality of the mix entering the chamber

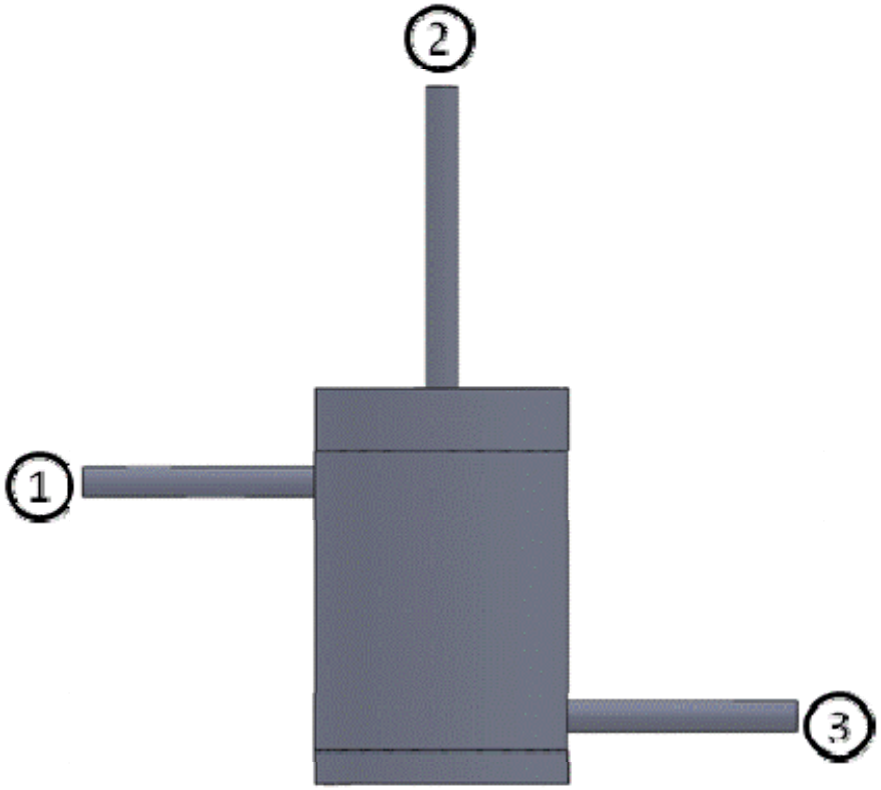

Figure 3.35. Cyclone 2-D model

2. Determined the density of the liquid vapor mix by using equation 3.9.

$$\rho_1 = \rho_2 + \rho_3 \quad \textbf{3.9}$$

ρ_2 and ρ_3 were interpolated from the properties of Novec-7000 ρ_v and ρ_l properties, respectively at 34°C.

3. Calculated the velocity of the liquid at point 3 in Figure 3.35 using equation 3.10 since the mass flow rate at that point was known

$$V = \frac{\dot{m}}{\rho A} \quad \textbf{3.10}$$

4. Determined P_1, P_2, and P_3 from the data acquisition system
5. Calculated the roots from the quadratic equation. The highest root will be the velocity of the fluid. The relationship was developed using the Bernoulli's and continuity equations

Bernoulli's equation is presented in equation 3.12 below:

$$\frac{P_1}{\rho_1} + \frac{v_1^2}{2} = \frac{P_2}{\rho_2} + \frac{v_2^2}{2} + \frac{P_3}{\rho_3} + \frac{v_3^2}{2} \quad \textbf{3.11}$$

Continuity:

$$\dot{m}_{in} = \dot{m}_{out} \quad \textbf{3.12}$$

$$\dot{m}_1 = \dot{m}_2 + \dot{m}_3 \quad \textbf{3.13}$$

$$\rho_1 V_1 A_1 = \rho_2 V_2 A_2 + \rho_3 V_3 A_3 \quad \textbf{3.14}$$

Solving the continuity equation for V_1 and knowing that: $A_1 = A_2 = A_3 = A$.

$$V_2 = \frac{\rho_1 V_1 A_1 - \rho_3 V_3 A_3}{\rho_2 A_2} = \frac{\rho_1 V_1 - \rho_3 V_3}{\rho_2} \quad \textbf{3.15}$$

Now plug V_2 into the Bernoulli equation:

$$\frac{P_1}{\rho_1} + \frac{v_1^2}{2} = \frac{P_2}{\rho_2} + \frac{1}{2}\left(\frac{\rho_1 V_1 - \rho_3 V_3}{\rho_2}\right)^2 + \frac{P_3}{\rho_3} + \frac{v_3^2}{2}$$

Now apply the quadratic equation to get v_2:

$$v_{1_{Roots}} = \frac{-b \pm \sqrt{b^2 - 4ac}}{2a} \quad \textbf{3.16}$$

$$a = \rho_2^2 + \rho_1^2$$

$$b = (2v_3\rho_1\rho_3)$$

$$c = \left[-2(\rho_2^2)\left(-\frac{P_2}{\rho_2} + \frac{P_3}{\rho_3} + \frac{v_3^2}{2} - \frac{P_1}{\rho_1}\right) - \left(v_3\rho_3\right)^2\right]$$

Since the number under the radical was negative, the number was imaginary so to determine the magnitude equation 3.17 was used as follows:

$$|z| = \sqrt{x^2 + y^2} \quad \textbf{3.17}$$

where,

$$x = \frac{-b}{2a}, \qquad \text{and} \qquad y = \frac{\sqrt{b^2 - 4ac}}{2a} i$$

$$|v_1| = \sqrt{\left(\frac{-b}{2a}\right)^2 + \left(\frac{\sqrt{b^2 - 4ac}}{2a}\right)^2} \quad \textbf{3.18}$$

Compare the quality reading from the void fraction sensor to the calculated data.

Pump

For the pump to be considered an acceptable component in the thermal loop, it had to be able to supply an adequate amount of fluid to the heated surface. An adequate amount of fluid would be an amount of fluid sufficient enough to cause the surface to reach a steady state temperature under maximum heat flux.

Heat Exchanger and Chiller

To classify the heat exchanger and chiller as components that benefit the performance of the thermal loop, the chiller had to receive the operator desired amount of energy and produce an operator desired amount of fluid quality. To determine acceptability the temperature change between the ambient air and the heat exchanger, the temperature change was measured and a relationship was determined to gauge the adequacy of the energy removal from the internal fluid.

CHAPTER 4

RESULTS AND DISCUSSION

The results obtained from the experiments performed on the removal of heat from a heater to a chiller were used to explain whether the individual components functioned properly. The following results were obtained using the test matrixes outlined in the previous chapter. The instrumentation used to gather the data in these experiments was designed by Hewlin (2010).

4.1 Validation of Heater Performance

Figure 4.1 shows the heating curve at a low, medium, and maximum heat flux at the maximum flow rate of 0.95 l/min. The temperature represented in the figure was measured at the heater surface.

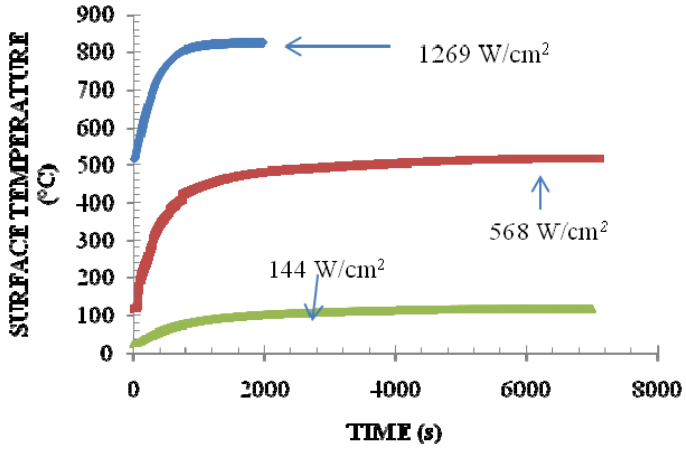

Figure 4.1. Heating curve at 0.95 l/min

From Figure 4.1, it can be seen that at the flow rate of 0.95 l/min the system was able to reach a steady state temperature for the following input heat fluxes; 1,269 W/cm^2, 568 W/cm^2, and 144 W/cm^2. The data also shows that it takes a significant amount of time for the system to reach a steady state temperature at the low and medium heat fluxes input. The time elapse was due to the fact that as the input heat flux increases the time required to reach steady state temperature decreased.

Figure 4.2 shows the heating curve created at the maximum heat flux and the minimum flow rate of 0.75 l/min.

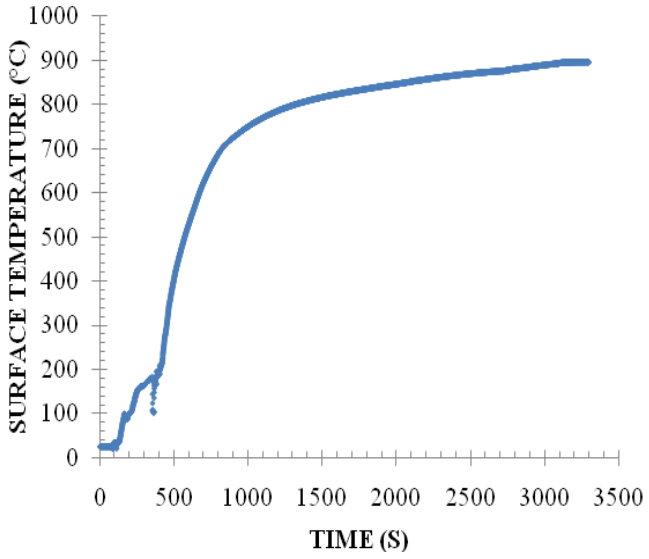

Figure 4.2. Heating curve at 0.75 l/min

From Figure 4.2, it is seen that the amount of liquid being supplied, described by the flow rate of 0.75 l/min, to the heated surface was insufficient at maintaining the

heater temperature at a constant value. From the experiment, it was determined that performing this test at a flow rate less than 0.75 l/min would be inadequate at removing a heat flux of 1,269 W/cm^2. This was determined by the observation of the cartridge heater wires glowing red during the test which resulted in the surface temperature reached 824 °C. As a result of the wires beginning to glow red, the test was stopped for safety reasons and the flow rate of 0.75 l/min was recorded as the minimum rate at which the flow loop would provide cooling without causing heater melt down. From the same experiment, it was also discovered that instantaneous application of the maximum voltage to the dc power supply would cause the over current protection switch to trip; thereby shutting the system down. To remedy this, the voltage should be applied gradually from a lower setting. The effects of the system shutdown can be seen in the first few hundred seconds. The data shows the temperature dips for a short time before it was restored by the system operator.

4.2 Validation of Pump Performance

In order to have a working fluid system there must be a pump to move that fluid. This section is devoted to discussing the results obtained from experiments that were carried out to determine the pumps functionality in the system.

Figure 4.3(a) and (b) show the actual voltage output from the proximity probe. This data is used to determine the speed of the pump as described in Chapter three. From Figure 4.3(a), it can be seen that as the shaft rotates the on/off function of the proximity

probe creates a step wave. Figure 4.3(b) shows a single period of the total elapsed time. From Figure 4.3 (b), the speed of the motor was determined to be 400 RPM.

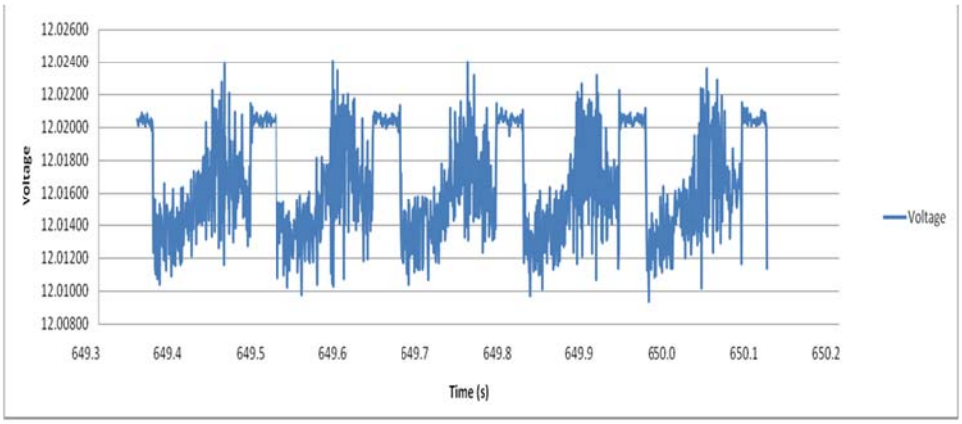

(a)

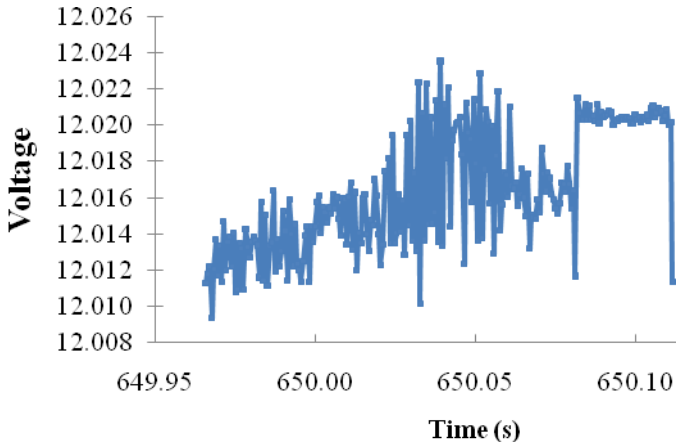

(b)

Figure 4.3. (a) Voltage versus Time for proximity probe (b) One period of the Voltage versus Time plot from part (a)

Figure 4.4 shows the direct relationship between the speed of the motor and the setting of the variable speed controller. From Figure 4.4, it can be seen that the variable

speed controller can increase the output speed of the motor in a linear manner. The minimum speed of the variable speed controller was set so that when it was turned on, the pump began moving the fluid through the loop. Initially, the controller was set such that when it was turned on, the pump would begin to turn, but this was an insufficient speed to cause the fluid to move through the pipes.

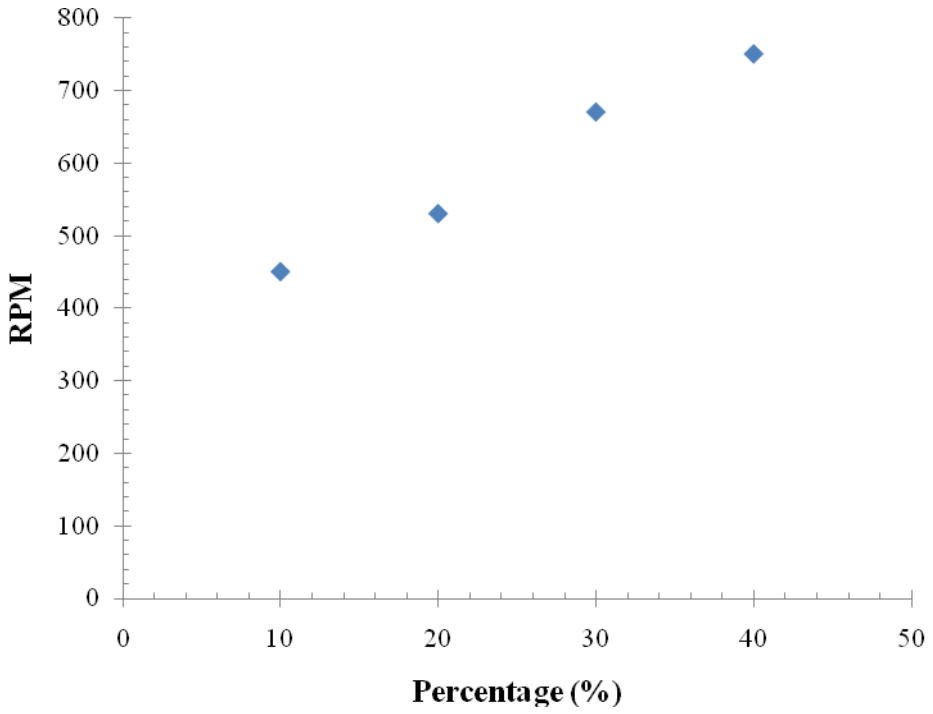

Figure 4.4. RPM versus Variable speed controller setting

Figure 4.5 shows the flow rates achieved at the inlet to the heater chamber relative to the setting of the DC speed controller. From Figure 4.5, it is seen that the minimum liquid flow rate that can be achieved was 0.80 l/min and the maximum was 0.85 l/min.

The figure also shows that after the variable speed controller is set to 30%, the pump speed has no effect on the flow rate of the fluid. After visual inspection of this phenomenon, it was concluded that the loss of pumping potential after 30% was possibly caused by system instability. The system instability was deduced from observing pulsing flow at higher speeds. Also, during the test, the mass flow rate in the system did not reach the maximum flow rate achieved during the initial test. The fact that the same flow rate could not be achieved was attributed to the amount of fluid that was put into the system.

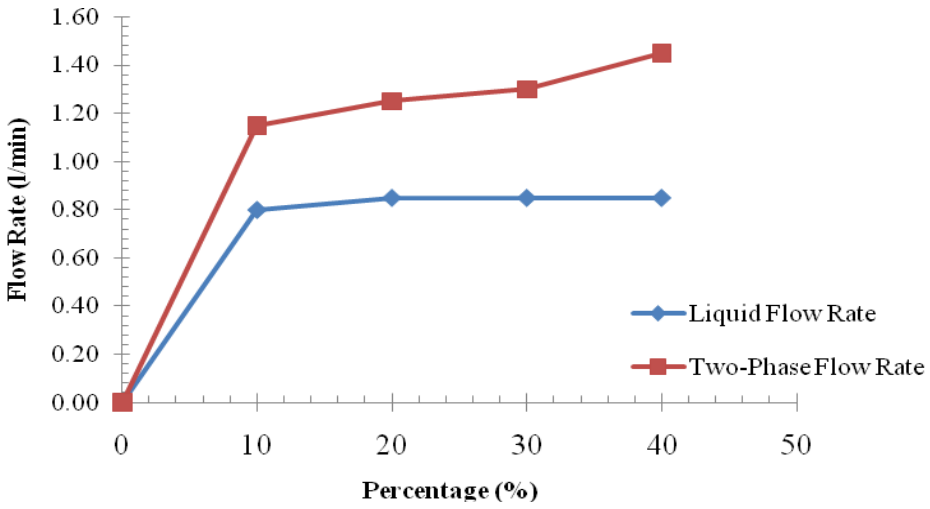

Figure 4.5. Flow Rate versus Speed Controller Setting

From the testing, it was observed that in order to determine the maximum flow rate of liquid into the chamber, the vapor line would have to be closed. By closing the vapor line, the flow rate into the chamber would no longer be divided between the liquid

and vapor lines, thus allowing for the maximum flow rate to be achieved in the liquid line.

4.3 Validation of Cyclone Performance

To determine whether the cyclone was functioning properly, a different methods where derived. Majority of the methods were discerned during the experimentation process. Figure 4.6 visually depicts the first method that was discerned during experimentation.

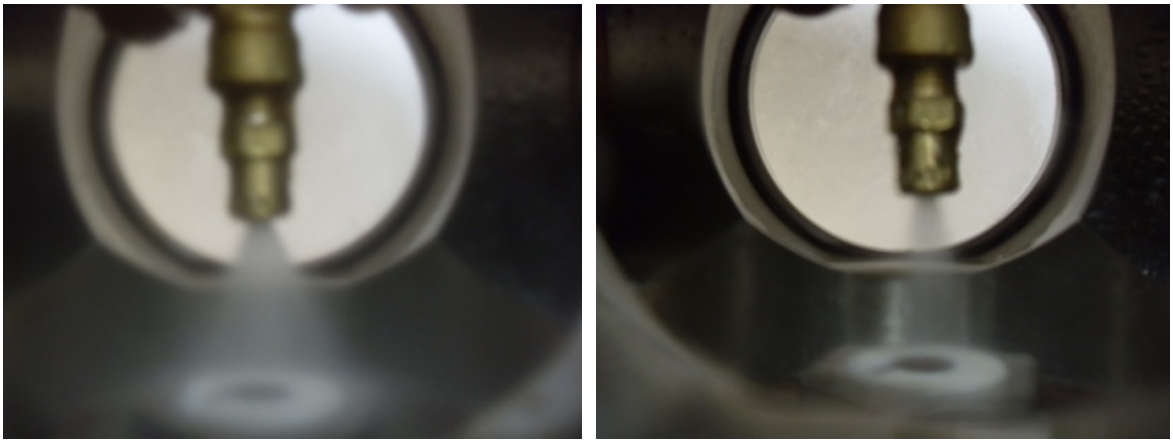

(a) (b)

Figure 4.6. (a) ¾ - 90 nozzle with a single phase flow (b) ¾ - 90 nozzle with a two-phase flow

From Figure 4.6, it can be seen that there was a significant difference between the spray cone shapes produced by a two-phase flow in comparison to that of a single-phase flow. The first method was derived by visualization of the different spray shapes in the presence of two-phase and single phase sprays from the same nozzle. The relationship

was discovered when different nozzle types were examined to determine which nozzle produced the best cone shape. From the characterization of the nozzles, it was determined that when a single phase was present the spray shape was defined but in the presence of two-phases the nozzle type had no major effect on the overall spray shape. In the case where two-phases are present, the spray shape was relatively the same regardless of the type of nozzle used as seen in Figure 4.7. Therefore, from Figure 4.6 and Figure 4.7, it can be concluded that the cyclone properly separates the two-phase mixture into its individual liquid and vapor components.

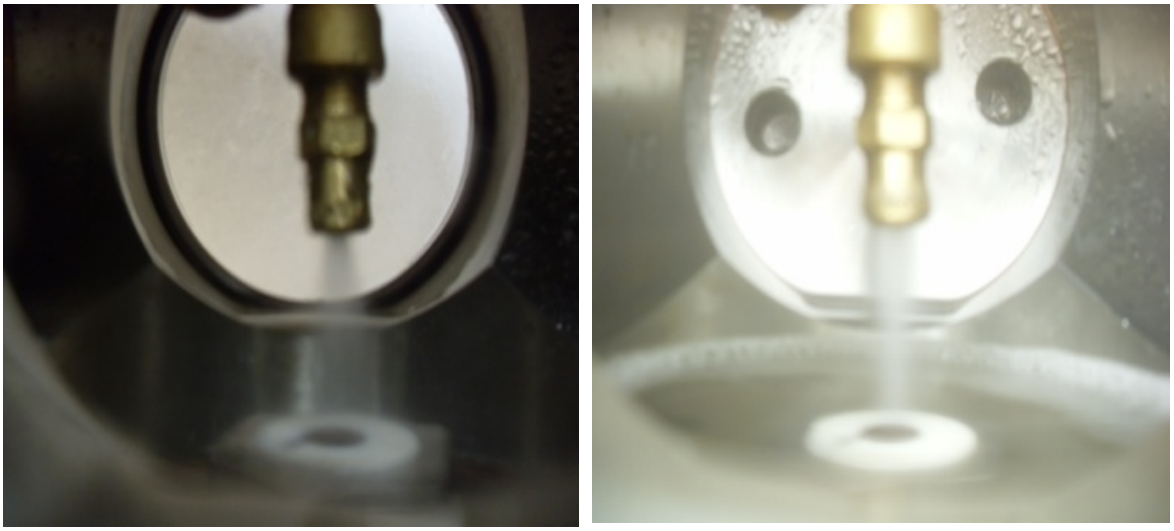

(a) (b)

Figure 4.7. (a) ¾ - 90 nozzle with two-phase flow (b) ½ - 90 nozzle with two-phase flow

Figure 4.8 shows another relationship obtained during experimentation which was the visualization of flow through the flow meter. From Figure 4.8 (a), it can be seen that in a two-phase flow with the vapor valve open, only the liquid phase passes through the

flow meter. Figure 4.8 (b) shows that when the vapor valve is closed, the liquid flow meter consist of a two-phase mixture. From these images it be concluded that the cyclone functions properly.

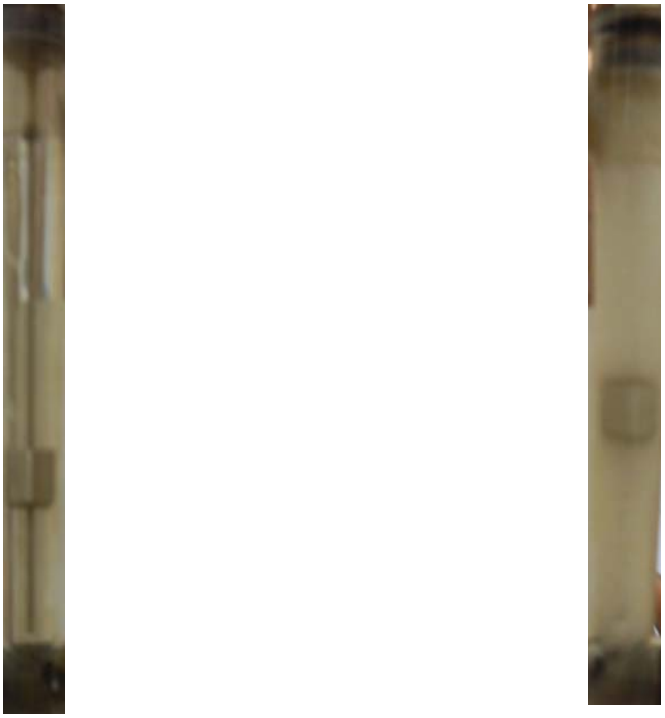

(a) (b)

Figure 4.8. (a) Flow meter with single-phase (b) Flow meter with two-phase dispersed bubbly flow

Table 4.1 shows the relationship between mass flow rate and pressure at the cyclone, which was the final method used to determine whether the cyclone was working. The table also shows that the flow rate of vapor is greater than the liquid when the liquid flow rate is 0.84 l/min. The mass flow rate for the mixture and the vapor were obtained

after the pressure transducers and the flow meter data obtained from the equations described in Chapter 3.

Table 4.1. Relationship between pressure and mass flow rate

Name	Location #	Pressure (MPa)	Mass flow rate (l/min)
Mix Inlet	1	0.2286	2.83
Vapor Outlet	2	0.2314	1.99
Liquid Outlet	3	0.2321	0.84

4.4 Validation of Heat Exchanger and Chiller Performance

Figure 4.9 shows the change in temperature of the heat exchangers from ambient when the chiller is running. Figure 4.9 shows the decrease in temperature of the inlet and outlets to the heat exchanger on the chiller side.

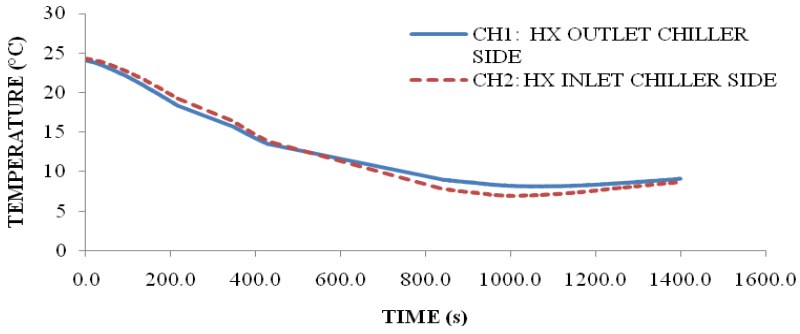

Figure 4.9. Temporal performance of the heat exchanger

The temperature of the chiller was set at 4.44 °C (40 °F). So from this figure, it can be seen that when the system is at room temperature, it takes about 15 minutes for the

temperature to reach its minimum setting. There was also a noticeable difference between the inlet and outlet temperature from the fluid absorbed from the surrounding environment. From this, it was concluded that the dual heat exchanger setup would adequately remove enough energy from any passing fluid.

4.5 Validation of Overall System Performance

Figure 4.10 shows the capability of the entire thermal loop to withstand a vacuum pressure. The plot describes the fact that the individual components are properly connected without any leakage. From Figure 4.10, it is seen that the system is capable of reaching a pressure of almost a -0.0800 MPa in about 5 min, and is capable of maintaining this pressure. After the system reached the lowest pressure, the vacuum pump was turned off and for the last 3.5 minutes the system was measured to see if it could maintain the pressure. The data shows that the system was capable of maintaining a negative pressure.

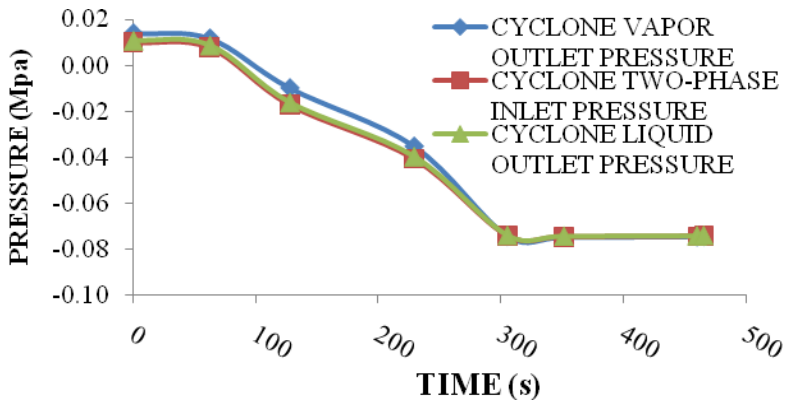

Figure 4.10. Temporal system pressure with an injector chamber subjected to vacuum

CHAPTER 5

CONCLUSION

5.1 Concluding Remarks

The data presented in the previous chapters showed that the design of the final system was a success. All the design requirements were met. The specific objectives were to:

1. Develop a system capable of removing a high heat flux in a two-phase spray cooling loop

2. Design components capable of removing high heat fluxes in a two-phase spray cooling loop

The overall goal and objectives were deemed successful because of the following observations:

1. The heater was able to reach a steady state temperature at the maximum heat flux,

2. The pump was able to supply enough fluid to cause the heater to reach a steady state temperature at the maximum heat flux,

3. The cyclone was able to separate a two-phase fluid into its individual liquid and vapor components,

4. The chiller and heat exchanger were able to remove enough energy from the fluid to reduce the fluid temperature,

5. All the individual components, once integrated to form a system were able to function as a unit to remove the maximum heat flux.

The system performed adequately for experimental input conditions imposed and if used as designed with the recommendations described below, the system will make an optimal platform for developing cooling flow studies in the future.

5.2 Recommendations

During the course of experimentation, minor obstacles arose which may require system modification to optimize performance. The following recommendations were developed.

1. The relocation of the accumulator could greatly increase the flow efficiency of the system. In the final design, the accumulator was setup as a bypass in the system. The implications were that if there was excess fluid in the system it would go to the accumulator or continue running through the loop bypassing the accumulator. The proposed modification to the current design requires relocating the accumulator to be in-line with the main flow path. All the fluid flow would now be routed through the accumulator. To determine the implications of the design changes, an electrical equivalency diagram was constructed.

    a. Created an electrical equivalency showing change in setup. Pump represents a voltage supply, and the accumulator can be represented as a capacitance/resistor electric model. The flow meter and piping can be represented as resistances.

    b. Electrical models showing the current and proposed component layout are shown in Figure 5.1 and Figure 5.2. Figure 5.1 shows the accumulator and flow meter as parallel resistors whereas Figure 5.2 shows them as a

series resistance combination. Before proceeding on the design, a numerical analysis must be performed to determine the optimal layout.

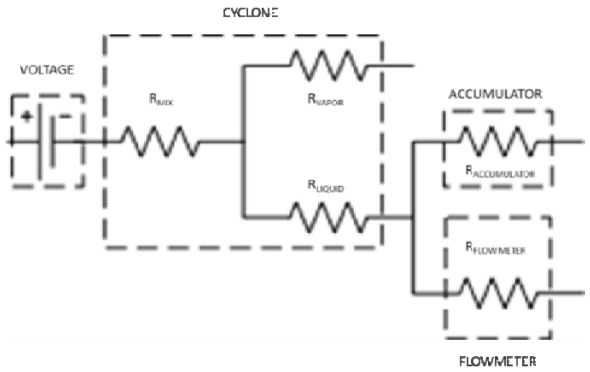

Figure 5.1. Electrical equivalent of current system setup

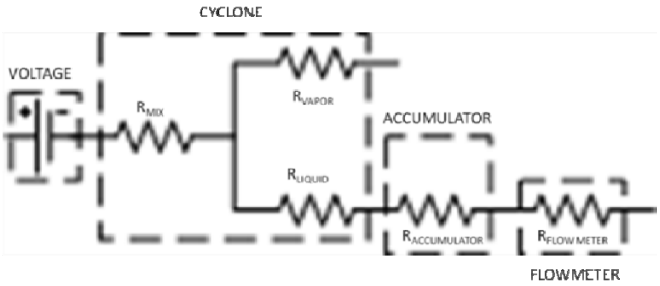

Figure 5.2. Electrical equivalent of proposed system setup

2. During experimentation stages on the current study, one of the glass view ports on the injector chamber ruptured under a pressure of 0.1724 MPa. After incident review, it was determined that the glass view ports that are capable of withstanding ultra high vacuum (UHV 10^{-8} torr or lower), were not designed for positive pressure. The observations were confirmed by the vendor; Kurt J. Lesker. Therefore, based the component manufacture recommendation, "Any

chamber equipped with a viewport must not be subject to a positive internal pressure," a component change for the future thermal loop must be performed. The current view ports are illustrated in Figure 5.3(a). After analysis of the current view port design, and researching pressure vessel view ports, it was determined that the rupture was due to the front side of the glass being unsupported. As a result, a recommendation was made that the current viewports be replaced with pressure vessel viewports shown in Figure 5.3(b). Specifically, the pressure vessel view ports are supported on both sides. Furthermore, the application of a Lexan shielding perimeter should be implemented around the heater/injector chamber.

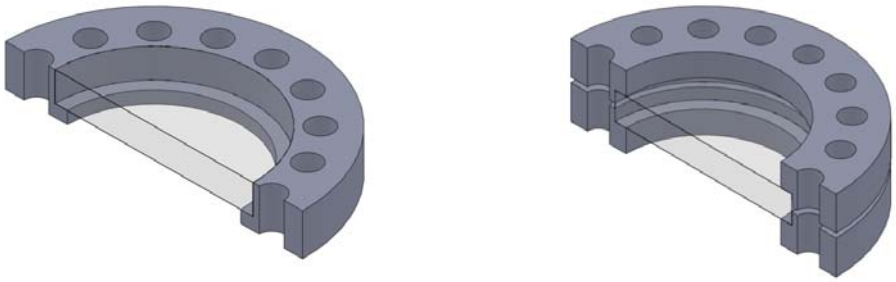

(a) (b)

Figure 5.3. (a) Schematic of a vacuum chamber view port, (b) Schematic of a pressure vessel view port

3. Another issue that arose during experimentation was a significant decrease in flow rate during high heat flux heater settings. The incident review revealed that hot fluid was entering the suction port of the pump. The temperature of the fluid exceeded the manufacturer recommended specification. Since the

manufacturer offers an upgraded stator made of a material capable of withstanding higher temperatures, the current stator should be replaced with the new type. In addition to the upgraded stator, cooling should be added to the drainage line to reduce the fluid temperature at the pump suction port.

4. During the running of a standalone experiment with the heater extension, the glass mica insulator cracked due to a rapid change in temperature. The cracking can be deterred by continuous cooling of the heater throughout the entire experimental studies. Or, possibly a different material should be selected.

5. During the assembly of the heater into the heater chamber, the amount of effort required was extensive. To reduce the effort, an access flange could be adapted to the current heater chamber to make accessibility easier.

On completion of these recommendations, the loop should be able to safely and adequately operate within a wide range of input parameters.

REFERENCES

Amon, C. H., Yao, S.-C., Wu, C.-F., & Hsieh, C.-C. (2005). "Microelectromechanical System-Based Evaporative Thermal Management of High Heat Flux Electronics," *Journal of Heat Transfer, 127*(1), 66-75.

Bostanci, H., Rini, D. P., Kizito, J. P., & Chow, L. C. (2009). "Spray Cooling With Ammonia on Microstructured Surfaces: Performance Enhancement and Hysteresis Effect," *Journal of Heat Transfer-Transactions of the ASME,* 131(7), p. 168.

Çengel, Y. A. (2007). Heat and mass transfer : a practical approach (3rd ed.). Boston: McGraw-Hill.

Çengel, Y. A., & Boles, M. A. (2002). Thermodynamics : an engineering approach (4th ed.). Boston: McGraw-Hill.

Chen, R. H., Chow, L. C., & Navedo, J. E. (2004). "Optimal spray characteristics in water spray cooling," *International Journal of Heat and Mass Transfer,* 47(23), 5095-5099.

Chizhov, A. V., & Takayama, K. (2004). "The impact of compressible liquid droplet on hot rigid surface," *International Journal of Heat and Mass Transfer,* 47(6-7), 1391-1401.

Coursey, J. S., Kim, J. G., & Kiger, K. T. (2007). "Spray cooling of high aspect ratio open microchannels," *Journal of Heat Transfer-Transactions of the ASME,* 129(8), 1052-1059.

Fabbri, M., Jiang, S. J., & Dhir, V. K. (2005). "A comparative study of cooling of high power density electronics using sprays and microjets," *Journal of Heat Transfer-Transactions of the ASME,* 127(1), 38-48.

Fox, R. W., & Mc Donald, A. T. (1985). Introduction to fluid mechanics, 3rd edition.

Graco et al., (2007) Technical Application Information, from http://www.graco.com/LCC/etoolbox/vacuum.html

Griffin, A. R., Vijayakumar, A., Chen, R. H., Sundaram, K. B., & Chow, L. C. (2008). "Development of a transparent heater to measure surface temperature fluctuations under spray cooling conditions," *Journal of Heat Transfer-Transactions of the ASME,* 130(11).

Horacek, B., Kiger, K. T., & Kim, J. (2005). "Single nozzle spray cooling heat transfer mechanisms," *International Journal of Heat and Mass Transfer,* 48(8), 1425-1438.

Hsieh, C. C., & Yao, S. C. (2006). "Evaporative heat transfer characteristics of a water spray on micro-structured silicon surfaces," I*nternational Journal of Heat and Mass Transfer,* 49(5-6), 962-974.

Hsieh, S. S., Fan, T. C., & Tsai, H. H. (2004). "Spray cooling characteristics of water and R-134a. Part 1: nucleate boiling," *International Journal of Heat and Mass Transfer, 47*(26), 5703-5712.

Hsieh, S. S., & Tien, C. H. (2007). "R-134a spray dynamics and impingement cooling in the non-boiling regime," *International Journal of Heat and Mass Transfer,* 50(3-4), 502-512.

Kim, J. H., You, S. M., & Choi, S. U. S. (2004). "Evaporative spray cooling of plain and microporous coated surfaces," *International Journal of Heat and Mass Transfer,* 47(14-16), 3307-3315.

Lin, L. C., & Ponnappan, R. (2003). "Heat transfer characteristics of spray cooling in a closed loop," *International Journal of Heat and Mass Transfer,* 46(20), 3737-3746.

Lin, L. C., Ponnappan, R., & Yerkes, K. (2006). "Actively pumped two-phase loop for spray cooling," *Journal of Thermophysics and Heat Transfer,* 20(1), 107-110.

Mudawar, I., Bharathan, D., Kelly, K., & Narumanchi, S. (2009). "Two-Phase Spray Cooling of Hybrid Vehicle Electronics," *IEEE Transactions on Components and Packaging Technologies,* 32(2), 501-512.

Mudawar, I., & Estes, K. A. (1996). "Optimizing and predicting CHF in spray cooling of a square surface," *Journal of Heat Transfer-Transactions of the ASME,* 118(3), 672-679.

Nikolopoulos, N., Theodorakakos, A., & Bergeles, G. (2007). "A numerical investigation of the evaporation process of a liquid droplet impinging onto a hot substrate," *International Journal of Heat and Mass Transfer,* 50(1-2), 303-319.

Oliphant, K., Webb, B. W., & McQuay, M. Q. (1998). "An experimental comparison of liquid jet array and spray impingement cooling in the non-boiling regime," *Experimental Thermal and Fluid Science,* 18(1), 1-10.

Ortiz, L., & Gonzalez, J. E. (1999). "Experiments on steady-state high heat fluxes using spray cooling," *Experimental Heat Transfer,* 12(3), 215-233.

Pais, M. R., Chow, L. C., & Mahefkey, E. T. (1992). "Surface-Roughness and Its Effects on the Heat-Transfer Mechanism in Spray Cooling," *Journal of Heat Transfer-Transactions of the ASME,* 114(1), 211-219.

Park, C., Vallury, A., Zuo, J., Perez, J., & Rogers, P. (2007). "Electronics Thermal Management Using Advanced Hybrid Two-Phase Loop Technology," *ASME Conference Proceedings,* 2007(42754), 911-916.

Pautsch, A. G., & Shedd, T. A. (2005). "Spray impingement cooling with single- and multiple-nozzle arrays. Part I: Heat transfer data using FC-72," *International Journal of Heat and Mass Transfer,* 48(15), 3167-3175.

Rybicki, J. R., & Mudawar, I. (2006). "Single-phase and two-phase cooling characteristics of upward-facing and downward-facing sprays," I*nternational Journal of Heat and Mass Transfer,* 49(1-2), 5-16.

Sellers, S. M., & Black, W. Z. (2008). "Boiling heat transfer rates for small precisely placed water droplets on a heated horizontal plate," *Journal of Heat Transfer-Transactions of the ASME, 130*(5), -.

Selvam, R. P., Lin, L. C., & Ponnappan, R. (2006). "Direct simulation of spray cooling: Effect of vapor bubble growth and liquid droplet impact on heat transfer," *International Journal of Heat and Mass Transfer*, 49(23-24), 4265-4278.

Shedd, T. A. (2007). "Next generation spray cooling: High heat flux management in compact spaces," *Heat Transfer Engineering,* 28(2), 87-92.

Tao, Y. J., Huai, X. L., & Li, Z. G. (2009). Numerical Simulation of Vapor Bubble Growth and Heat Transfer in a Thin Liquid Film. Chinese Physics Letters, 26(7), -.

Visaria, M., & Mudawar, I. (2009). "Application of Two-Phase Spray Cooling for Thermal Management of Electronic Devices," I*EEE Transactions on Components and Packaging Technologies,* 32(4), 784-793.

Yang, J., Chow, L. C., & Pais, M. R. (1996). "Nucleate boiling heat transfer in spray cooling," *Journal of Heat Transfer-Transactions of the ASME,* 118(3), 668-671.

APPENDIX A

PUMP CALCULATIONS

$$\dot{E}_{liquid} + \dot{E}_{source} = \dot{E}_{vapor}$$

$$\dot{Q}_l + \dot{Q}_s = \dot{Q}_v$$

$$\dot{Q}_s = \dot{m}_v h_{fg} - \dot{m}_l c_p \Delta T$$

$$\dot{Q}_s = \dot{m}(h_{fg} - c_p \Delta T)$$

$$\dot{m} = \frac{\dot{Q}_s}{h_{fg} - c_p \Delta T}$$

$$\dot{V} = \frac{\dot{m}}{\rho}$$

$$c_p = 1.300 \frac{kJ}{kg \cdot °C}$$

$$\rho = 1400 \frac{kg}{m^3}$$

$$h_{fg} = 142 \frac{kJ}{kg}$$

$T_2 = 34°C,$ Boling point

$T_1 = 25°C,$ Saturation Temperature

$$\dot{Q} = 1000 \frac{W}{cm^2} = 1 \frac{kJ}{s}$$

And

$$\dot{Q} = 4000 \frac{W}{cm^2} = 4 \frac{kJ}{s}$$

You get,

$$\dot{m}_{1000} = 7.675 \times 10^{-3} \frac{kg}{s}$$

$$\dot{V}_{1000} = 5.482 \times 10^{-6} \frac{m^3}{s}$$

for a heat flux of 1000 W which,

$$\dot{V}_{1000} = 0.0869 \; GPM$$

and

$$\dot{m}_{4000} = 3.0698 \times 10^{-2} \frac{kg}{s}$$

$$\dot{V}_{4000} = 2.193 \times 10^{-5} \frac{m^3}{s}$$

for a heat flux of 4000 W which, $= 0.3476 \; GPM$

APPENDIX B

HEAT EXCHANGER

$$\dot{Q} = [\dot{m} c_p (T_{out} - T_{in})]_{cooling} = (\dot{m} h_{fg})_{vapor}$$

$$\dot{Q} = (\dot{m} h_{fg})_{vapor}$$

$$h_{fg@34°C} = \frac{(34-20)(233-207)}{(40-20)} + 207 = 218.2 \frac{kJ}{kg}$$

$$\dot{Q}_{4000} = (3.0698 \times 10^{-2})(218.2) = 6.698 \frac{kJ}{s}$$

$$= 22,861 \frac{Btu}{hr}$$

$$\dot{Q}_{1000} = 1.675 \frac{kJ}{s} = 5,715.7 \frac{Btu}{hr}$$

$$\dot{m} = \frac{\dot{Q}}{c_p \Delta T}$$

$$\dot{m} = \frac{6.698}{(4.194)(10)} = 0.1597 \frac{kg}{s}$$

$$= 2.531 gpm$$

$$\dot{m}_{1000} = 0.03993 \frac{kg}{s} = 0.6329 gpm$$

And if you interpolate, the specific heat for Ethylene Glycol (Antifreeze) $c_p = 3.349 \frac{kJ}{kg \cdot °C}$, and still assuming a change in temp of 10 degrees and then,

$$\dot{m}_{4000} = 0.2 \frac{kg}{s} = 3.17 gpm$$

And

$$\dot{m}_{1000} = 0.05 \frac{kg}{s} = 0.7928 gpm$$

APPENDIX C

HEATER/INJECTOR CHAMBER

$$\dot{Q}_{emitted} = \varepsilon \sigma A_s T_s^4$$

Where,

$$\varepsilon_{copper} = 0.03$$

$$\sigma = 5.67 \times 10^{-8}$$

$$A_s = 0.01117\ m^2$$

$$T_s = 400 + 273 = 673K$$

$$\dot{Q}_{emitted@400°C} = (0.03)(5.67 \times 10^{-8})(0.01117)(673)^4 = 3.898\ W$$

And if $T_s = 800 + 273 = 1073K$

$$\dot{Q}_{emitted@800°C} = 25.186\ W$$

$$\dot{Q}_{absorbed} = \alpha \dot{Q}_{emitted}$$

So from the calculations it was determined that the material that absorbs the least amount of energy is polished aluminum. What this data say's is that if a heater block emitted 25.186 Watts in the form of radiation the polished aluminum lining would only absorb 2.267 Watts of that energy meaning that it would reflect 22.919 Watts back to the block.